Monthly Notices of the ROYAL ASTRONOMICAL SOCIETY

MNRAS **459,** 1764–1780 (2016) doi:10.1093/mnras/stw630
Advance Access publication 2016 March 17

Next generation cosmology: constraints from the *Euclid* galaxy cluster survey

B. Sartoris,[1,2]★ A. Biviano,[2] C. Fedeli,[3,4] J. G. Bartlett,[5] S. Borgani,[1,2,6] M. Costanzi,[7] C. Giocoli,[3,4,8,9] L. Moscardini,[3,4,8] J. Weller,[7,10,11] B. Ascaso,[5,12] S. Bardelli,[3] S. Maurogordato[13] and P. T. P. Viana[14,15]

[1]*Dipartimento di Fisica, Sezione di Astronomia, Università di Trieste, Via Tiepolo 11, I-34143 Trieste, Italy*
[2]*INAF/Osservatorio Astronomico di Trieste, Via Tiepolo 11, I-34143 Trieste, Italy*
[3]*INAF/Osservatorio Astronomico di Bologna, Via Ranzani 1, I-40127 Bologna, Italy*
[4]*INFN, Sezione di Bologna, Viale Berti Pichat 6/2, I-40127 Bologna, Italy*
[5]*APC, AstroParticule et Cosmologie, Université Paris Diderot, CNRS/IN2P3, CEA/lrfu, Observatoire de Paris, Sorbonne Paris Cité, 10 rue Alice Domon et Léonie Duquet, F-75205 Paris Cedex 13, France*
[6]*INFN, Sezione di Trieste, Via Valerio 2, I-34127 Trieste, Italy*
[7]*Universitäts-Sternwarte München, Fakultät für Physik, Ludwig-Maximilians Universität München, Scheinerstr. 1, D-81679 Munchen, Germany*
[8]*Dipartimento di Fisica e Astronomia, Alma Mater Studiorum Università di Bologna, viale Berti Pichat 6/2, I-40127 Bologna, Italy*
[9]*Aix Marseille Université, CNRS, LAM (Laboratoire d'Astrophysique de Marseille) UMR 7326, F-13388 Marseille, France*
[10]*Excellence Cluster Universe, Boltzmannstr. 2, D-85748 Garching, Germany*
[11]*Max Planck Institute for Extraterrestrial Physics, Giessenbachstr. 1, D-85748 Garching, Germany*
[12]*GEPI, Observatoire de Paris, CNRS, Université Paris Diderot, 61 Avenue de l'Observatoire, F-75014 Paris, France*
[13]*Laboratoire J.-L. LAGRANGE, CNRS/UMR 7293, Observatoire de la Côte d'Azur, Université de Nice Sophia-Antipolis, F-06304 Nice Cedex 4, France*
[14]*Instituto de Astrofísica e Ciências do Espaço, Universidade do Porto, CAUP, Rua das Estrelas, P-4150-762 Porto, Portugal*
[15]*Departamento de Física e Astronomia, Faculdade de Ciências, Universidade do Porto, Rua do Campo Alegre 687, P-4169-007 Porto, Portugal*

Accepted 2016 March 14. Received 2016 March 14; in original form 2015 May 11

ABSTRACT

We study the characteristics of the galaxy cluster samples expected from the European Space Agency's *Euclid* satellite and forecast constraints on parameters describing a variety of cosmological models. In this paper we use the same method of analysis already adopted in the *Euclid Red Book*, which is based on the Fisher matrix approach. Based on our analytical estimate of the cluster selection function in the photometric *Euclid* survey, we forecast the constraints on cosmological parameters corresponding to different extensions of the standard Λ cold dark matter model. Using only *Euclid* clusters, we find that the amplitude of the matter power spectrum will be constrained to $\Delta\sigma_8 = 0.0014$ and the mass density parameter to $\Delta\Omega_{\rm m} = 0.0011$. The dynamical evolution of dark energy will be constrained to $\Delta w_0 = 0.03$ and $\Delta w_a = 0.2$ with free curvature Ω_k, resulting in a (w_0, w_a) figure of merit (FoM) of 291. In combination with *Planck* cosmic microwave background (CMB) constraints, the amplitude of primordial non-Gaussianity will be constrained to $\Delta f_{\rm NL} \simeq 6.6$ for the local shape scenario. The growth factor parameter γ, which signals deviations from general relativity, will be constrained to $\Delta\gamma = 0.02$, and the neutrino density parameter to $\Delta\Omega_\nu = 0.0013$ (or $\Delta\sum m_\nu = 0.01$). Including the *Planck* CMB covariance matrix improves dark energy constraints to $\Delta w_0 = 0.02$, $\Delta w_a = 0.07$, and a FoM = 802. Knowledge of the observable–cluster mass scaling relation is crucial to reach these accuracies. Imaging and spectroscopic capabilities of *Euclid* will enable internal mass calibration from weak lensing and the dynamics of cluster galaxies, supported by external cluster surveys.

Key words: galaxies: clusters: general – cosmological parameters – cosmology: theory – dark energy – large-scale structure of Universe.

1 INTRODUCTION

According to the hierarchical scenario for the formation of cosmic structures, galaxy clusters are the latest objects to have formed from

★ E-mail: sartoris@oats.inaf.it

the collapse of high density fluctuations filtered on a typical scale of ∼10 comoving Mpc (e.g. Kravtsov & Borgani 2012). Since galaxy clusters provide information on the growth history of structures and on the underlying cosmological model in many ways (see e.g. Allen, Evrard & Mantz 2011), they have played an important role in delineating the current standard Λ cold dark matter (ΛCDM) cosmological model. As a matter of fact, the number counts (NC) and spatial distribution of these objects have a strong dependence on a number of cosmological parameters, especially the amplitude of the mass power spectrum (PS) and the matter content of the Universe. The evolution with redshift of the cluster number density and correlation function can be employed to break the degeneracy between these two parameters, and thus can provide constraints on the cold dark matter (DM) and dark energy (DE) density parameters (e.g. Wang & Steinhardt 1998; Haiman, Mohr & Holder 2001; Weller, Battye & Kneissl 2002; Battye & Weller 2003; Allen et al. 2011; Sartoris et al. 2012). Furthermore, a number of studies (e.g. Carbone et al. 2012; Costanzi et al. 2013a, 2014) have also shown that clusters can be used to constrain neutrino properties, because massive neutrinos would directly influence the growth of cosmic structure, by suppressing the matter PS on small scales. More generally, since the evolution of the cluster population traces the growth rate of density perturbations, large surveys of clusters extending over a wide redshift interval have the potential of providing stringent constraints on any cosmological model whose deviation from ΛCDM leaves its imprint on this growth.

Over the past decade, surveys of galaxy clusters for cosmological use have been constructed and analysed, based on observations at different wavelengths: X-ray (e.g. Borgani et al. 2001; Vikhlinin et al. 2009; Clerc et al. 2012; Rapetti et al. 2013), sub-mm, through the Sunyaev & Zeldovich (1972) distortion (SZ henceforth; Staniszewski et al. 2009; Burenin & Vikhlinin 2012; Benson et al. 2013; Planck Collaboration XX 2014a), and optical (Rozo et al. 2010) bands. Further improvements can be obtained from the spatial clustering of galaxy clusters (Schuecker et al. 2003; Hütsi 2010; Mana et al. 2013). The resulting cosmological constraints turn out to be complementary to those of other cosmological probes such as Type Ia supernovae (e.g. Betoule et al. 2014), cosmic microwave background (CMB) radiation (e.g. Hinshaw et al. 2013; Planck Collaboration XVI 2014), the baryon acoustic oscillations (BAOs; e.g. Anderson et al. 2014), and cosmic shear (e.g. Basse et al. 2014; Kitching et al. 2014). These cluster catalogues are however characterized either by a large number of objects that cover a relatively small redshift range, or rather small samples that span a wide redshift range. Ideally, in order to exploit the redshift leverage with good statistics, one should have access to a survey that can provide a high number of well characterized clusters over a wide redshift range.

One future mission that will achieve this goal will be the European Space Agency (ESA) Cosmic Vision mission *Euclid*[1] (Laureijs et al. 2011). Planned for launch in the year 2020, *Euclid* will study the evolution of the cosmic web up to redshift $z \sim 2$. Although the experiment is optimized for the measurement of cosmological weak lensing (WL, or cosmic shear) and the galaxy clustering, *Euclid* will also provide data usable for other important complementary cosmological probes, such as galaxy clusters. Cluster detection will be possible in three different ways: (i) using photometric data; (ii) using spectroscopic data; and (iii) through gravitational (mostly weak) lensing, which may be combined for more efficiency. In this paper, we will perform our analyses by using the photometric cluster survey (see Section 2), where the cluster detection method is not dissimilar from that used to detect low-redshift Sloan Digital Sky Survey (SDSS) clusters (Koester et al. 2007). However, thanks to the use of near-infrared (NIR) bands, *Euclid* will be capable of detecting clusters at much higher redshifts ($z \sim 2$) over a similarly large area. The sky coverage of *Euclid* will reach 15 000 deg^2, almost the entire extragalactic celestial sphere. The characteristics of the *Euclid* spectroscopic survey and its possible use for the calibration of the mass–observable relation will be discussed in Appendices A and B, respectively.

One fundamental step for the cosmological exploitation of galaxy clusters is the definition of the relation between the mass of the host DM halo and a suitable observable quantity (e.g. Andreon & Hurn 2012; Giodini et al. 2013). Many efforts have been devoted to the calibration of the observable–mass scaling relations at different wave bands (e.g. Arnaud et al. 2010; Planck Collaboration XI 2011; Reichert et al. 2011; Rozo et al. 2011, 2014; Rykoff et al. 2012; Ettori 2013; Mantz et al. 2015; Wen & Han 2015) and in the definition of mass proxies which are at the same time precise (i.e. characterized by a small scatter in the scaling against cluster mass) and robust (i.e. relatively insensitive to the details of cluster astrophysics) (e.g. Kravtsov, Vikhlinin & Nagai 2006). In the case of *Euclid*, an internal mass calibration will be performed through the exploitation of spectroscopic and WL data of the wide *Euclid* survey (see Appendix B), and of the deep *Euclid* survey of 40 deg^2, 2 mag deeper than the wide survey. The deep survey will be particularly useful in adding constraints on the evolution of the observable–mass scaling relation at $z > 1$.

These *Euclid* internal data will provide a precise calibration of the relation between cluster richness, which characterizes photometrically identified clusters, and their actual mass. Furthermore, it will be possible to cross-correlate *Euclid* data with data from other cluster surveys – such as Extended Roentgen Survey with an Imaging Telescope Array (eROSITA; Merloni et al. 2012), XMM Cluster Survey (XCS; Mehrtens et al. 2012), the South Pole Telescope (SPT; Carlstrom et al. 2011), and the Atacama Cosmology Telescope (ACT; Marriage et al. 2011) – to further improve the mass calibration of *Euclid* clusters.

The aim of this paper is to forecast the strength and the peculiarity of the *Euclid* cluster sample in constraining the parameters describing different classes of cosmological models that deviate from the concordance ΛCDM paradigm. We first consider the case of a dynamical evolution of the DE component, using the two-parameter functional form originally proposed by Chevallier & Polarski (2001) and Linder (2003). The same parametrization has been used in the Dark Energy Task Force (DETF) reports (Albrecht et al. 2006, 2009) to estimate the constraining power of different cosmological experiments. Second, we allow for the primordial mass density perturbations to have a non-Gaussian distribution. Third, we explore the effect of deviations from general relativity (GR) on the linear growth of density perturbations. Finally, we consider the case of including massive standard neutrinos.

The structure of this paper is the following. In Section 2, we describe the approach used to estimate the *Euclid* cluster selection function of the photometric survey. In Section 3, we describe the Fisher matrix (FM) approach used to derive constraints from the *Euclid* cluster survey on cosmological parameters. In Section 4, we briefly describe the characteristics of the different cosmological models we consider. In Section 5, we show our results on the number of clusters that the wide *Euclid* survey is expected to detect as a function of redshift and the constraints that will be obtained

[1] http://www.euclid-ec.org

on the cosmological parameters using the cluster number density and PS. Finally, we provide our discussion and conclusions in Section 6. We present the analytical derivation of the spectroscopic selection function in Appendix A and the calibration of the cluster observable–mass relation in Appendix B.

2 GALAXY CLUSTER SELECTION IN THE *EUCLID* PHOTOMETRIC SURVEY

In this section, we adopt the cosmological parameter values of the concordance ΛCDM model from Planck Collaboration XVI (2014), $H_0 = 67\,\mathrm{km\,s^{-1}\,Mpc^{-1}}$ for the Hubble constant, $\Omega_\mathrm{m} = 0.32$ for the present-day matter density parameter, and $\Omega_k = 0$ for the curvature parameter.

To determine the selection function of galaxy clusters in the *Euclid* photometric survey, we adopt a phenomenological approach. We start by adopting an average universal luminosity function (LF) for cluster galaxies. Lin, Mohr & Stanford (2003) evaluated the K_s-band LFs of cluster galaxies out to a radius $r_{500,\mathrm{c}}$ for several nearby clusters. The radius r_Δ is defined as the radius of the sphere that encloses an average mass density Δ times the critical density of the Universe at the cluster redshift. These cluster LFs were parametrized using Schechter functions (Schechter 1976). We adopt the averages of the normalizations and characteristic luminosities listed in table 1 of Lin et al. (2003) for the 27 nearby clusters included in that analysis, corresponding to $\phi^\star = 6.4\ \mathrm{Mpc^{-3}}$ and $M^\star = -24.85$. Also, following Lin et al. (2003), we use a faint-end slope $\alpha = -1.1$, as confirmed in the r-band deep spectroscopic analysis of two nearby clusters by Rines & Geller (2008).

Concerning the behaviour of the cluster LF at $z > 0$, there is no conclusive observational evidence on the evolution of the LF faint-end slope parameter α (Mancone et al. 2012; Stefanon & Marchesini 2013). Therefore, we assume it to be redshift invariant. Also, the observed constancy of the richness versus mass relation for clusters up to $z \simeq 0.9$ (Lin et al. 2006; Poggianti et al. 2010; Andreon & Congdon 2014) suggests that there is no redshift evolution of $\phi^\star$, apart from the cosmological evolution of the critical density, which scales as $H^2(z)$.

We assume the $M^\star$ parameter to change with z according to passive evolution models of stellar populations (Kodama & Arimoto 1997). This assumption is justified because emission in the K_s band is not strongly influenced by young stellar generations, and it is supported by observations (Mancone et al. 2012, and references therein), at least for clusters more massive than $\sim 10^{14}\,\mathrm{M_\odot}$. For clusters of lower mass, some high-z surveys have found evidence for deviation from passive evolution of $M^\star$ (Mancone et al. 2010; Tran et al. 2010; Brodwin et al. 2013). However, the current observational evidence does not allow us to precisely parametrize $M^\star$ evolution to $z > 1$ and low cluster masses, and we prefer to keep our conservative assumption of passive evolution over the full cluster mass range.

We apply the early-type k-correction of Mannucci et al. (2001) to the $M^\star$ magnitudes. This correction should be the most appropriate for galaxies in clusters, which are mostly early type even at relatively high redshifts (Postman et al. 2005; Smith et al. 2005). We finally convert the K_s magnitudes into the *Euclid* band H_AB using the mean rest-frame colour for cluster galaxies, $H - K_\mathrm{s} = 0.26$ (we average the values provided by Boselli et al. 1997; de Propris et al. 1998; Ramella et al. 2004), and adopting the transformation to the AB-system $H_\mathrm{AB} = H + 1.37$ (Ciliegi et al. 2005). We thus obtain the cluster LFs in the H_AB band at different redshifts.

By integrating these LFs down to the apparent magnitude limit of the wide *Euclid* photometric survey ($H_\mathrm{AB} = 24$; see Laureijs et al. 2011), we then evaluate $n_{500,\mathrm{c}}$, namely the redshift-dependent number density of cluster galaxies within $r_{500,\mathrm{c}}$. The number of cluster galaxies contained within a sphere of radius $r_{500,\mathrm{c}}$ (i.e. the cluster richness) is then $N_{500,\mathrm{c}} = 4\pi\, n_{500,\mathrm{c}} r^3_{500,\mathrm{c}}/3 = 8/3\pi\, n_{500,\mathrm{c}} G M_{500,\mathrm{c}}/[500 H^2(z)]$, where the last equivalence follows from the relation between $r_{500,\mathrm{c}}$ and $M_{500,\mathrm{c}}$, the mass within a mean overdensity of 500 times the critical density of the Universe at the cluster redshifts. Note that the dependence of $N_{500,\mathrm{c}}$ on $H^{-2}(z)$ is only apparent, since $\phi^\star$, and hence $n_{500,\mathrm{c}}$, scales as $H^2(z)$. The z-dependence only comes in as a result of the fixed magnitude limit of the survey and the passive evolution of galaxies. In Fig. 1 we show $N_{500,\mathrm{c}}(z)$ for clusters of three different masses: $\log M_{200,\mathrm{c}} = 13.5, 14.0$, and 14.5 (black curves). To convert from $M_{500,\mathrm{c}}$ to $M_{200,\mathrm{c}}$ we adopt a Navarro–Frenk–White (NFW) profile (Navarro, Frenk & White 1997) with a mass- and redshift-dependent concentration given by the relation of De Boni et al. (2013, second relation from top in their table 5).

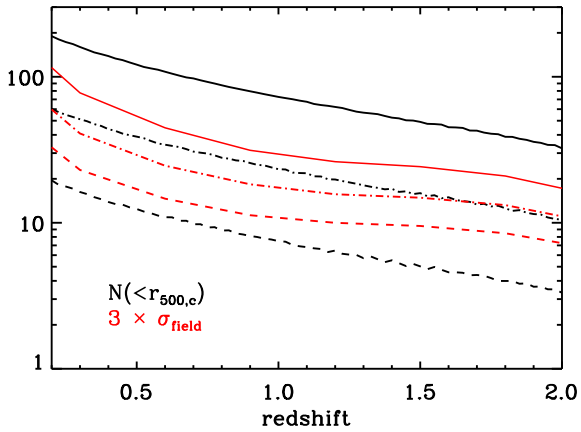

Figure 1. Number $N_{500,\mathrm{c}}$ of cluster galaxies within $r_{500,\mathrm{c}}$ (black curves), and $3\sigma_\mathrm{field}$, where σ_field is the rms of the field counts within the same radius, and within the adopted $3\Delta z_\mathrm{p}$ cut (red curves). These counts are shown down to the limiting magnitude of the *Euclid* survey, $H_\mathrm{AB} = 24$, as a function of redshift for clusters of different masses, $\log(M_{200,\mathrm{c}}/\mathrm{M_\odot}) = 14.5, 14.0, 13.5$ (solid, dot–dashed, dashed line, respectively), where masses are defined with a mean overdensity of 200 times the critical density of the Universe at the cluster redshifts.

We then estimate the contamination by field galaxies in the cluster area. We take the estimate of the number density of field galaxies down to $H_\mathrm{AB} = 24$ from the H-band counts of Metcalfe et al. (2006, see their table 3), $n_\mathrm{field} \simeq 33\ \mathrm{arcmin^{-2}}$, an estimate that is in agreement with the *Euclid* survey requirements (Laureijs et al. 2011). Multiplying this density by the area subtended by a galaxy cluster at any given redshift we obtain the number of field galaxies that contaminate the cluster field-of-view, $N_\mathrm{field} = n_\mathrm{field}\,\pi r^2_{500,\mathrm{c}}$, where $r_{500,\mathrm{c}}$ is in arcmin.

The number of field contaminants can be greatly reduced by using photometric redshifts, z_p. These will be obtained to the required accuracy of $\Delta z_\mathrm{p} \equiv 0.05(1 + z_\mathrm{c})$, by combining the *Euclid* photometric survey with auxiliary ground-based data (Laureijs et al. 2011). One can safely consider as non-cluster members all those galaxies that are more than $3\Delta z_\mathrm{p}$ away from the mean cluster redshift z_c. The mean cluster redshift will be evaluated by averaging the photometric redshifts of galaxies in the cluster region, and additionally including the (few) spectroscopic galaxy redshifts provided by the *Euclid* spectroscopic survey (see Appendix A).

In order to determine the fraction of field galaxies, $f(z_\mathrm{c})$, with photometric redshift z_p in the range $\pm 3 \times 0.05(1 + z_\mathrm{c})$ at any

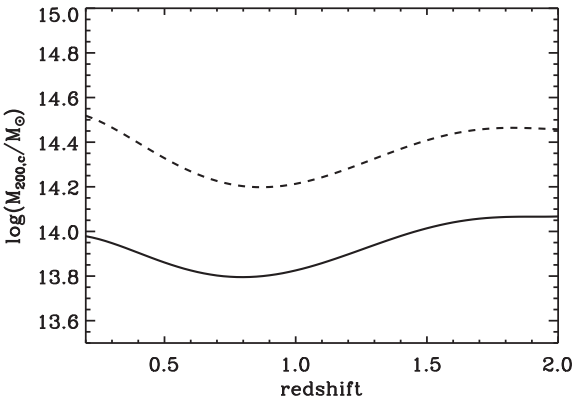

Figure 2. Galaxy cluster mass selection function for the *Euclid* photometric survey. Solid and dashed lines are for detection thresholds $N_{500,c}/\sigma_{\rm field} = 3$ and 5, respectively.

given z_c, we need to estimate the photometric redshift distribution of an $H_{AB} = 24$ limited field survey. To this aim we consider the photometric redshift distribution of galaxies with $H_{AB} \leq 24$ in the catalogue of Yang et al. (2014). We find $f(z_c) = 0.07, 0.23, 0.34$, and 0.33 at $z_c = 0.2, 0.8, 1.4$, and 2.0, respectively.

Finally, we evaluate the rms, $\sigma_{\rm field}$, of the field galaxy counts $f(z_c)N_{\rm field}$, by taking into account both Poisson noise and cosmic variance. For the latter we use the IDL code QUICKCV of John Moustakas[2] for cosmic variance calculation. In Fig. 1 we show $3\sigma_{\rm field}$ as a function of redshift, in clusters of $\log M_{200,c} = 13.5, 14.0$, and 14.5.

The ratio between the cluster galaxy NC and the field rms, $N_{500,c}/\sigma_{\rm field}$, gives the significance of the detection for a given cluster. The cluster selection function is the limiting cluster mass as a function of redshift for a given detection threshold. This is shown in Fig. 2 for two thresholds, $N_{500,c}/\sigma_{\rm field} = 3$ and 5. This selection function is only mildly dependent on redshift. The limiting cluster mass for the lowest selection threshold ($N_{500,c}/\sigma_{\rm field} = 3$) is $M_{200,c} \sim 8 \times 10^{13}\,{\rm M}_\odot$, lower than the typical mass of richness class 0 clusters in the Abell, Corwin & Olowin (1989) catalogue (Popesso et al. 2012). It is also similar to the limiting mass of the selection function of SDSS clusters identified by the maxBCG algorithm (see fig. 3 in Rozo et al. 2010), and to the typical mass of the clusters identified by Brodwin et al. (2007) up to $z \sim 1.5$ using z_p in an IR-selected galaxy catalogue. Preliminary tests based on running cluster finders on *Euclid* mocks[3] show that the mass limit $M_{200,c} \sim 8 \times 10^{13}\,{\rm M}_\odot$ roughly corresponds to ∼80 per cent completeness at all redshifts $z \leq 2$.

The shape of the selection functions shown in Fig. 2 is somewhat counter-intuitive because it is higher at $z \sim 0.2$ than at $z \sim 0.7$. Naively one would expect that clusters of lower mass would be easier to detect at lower redshifts. We find that this shape is related to the relative importance of cosmic variance and Poisson noise in the contaminating field counts. Cosmic variance drives the shape of the selection function at $z < 0.5$ and Poisson noise at higher redshifts. If we select clusters at a higher overdensity (e.g. $\Delta_c = 2500$ rather than $\Delta_c = 500$), the relative importance of cosmic variance and Poisson noise changes in a way to flatten the selection function at $z < 0.5$. In reality, observers do not select clusters at given Δ_c, so our estimate of the selection function must be considered only as an approximation. At the end of Section 5 we comment on the effect of taking a flat selection function out to $z = 2$.

So far we have not considered projection effects in the estimate of the selection function. These might in principle be important, as they cause confusion in the cluster identification, lowering the purity of the sample. In the specific case of the *Euclid* survey presented here, however, they are unlikely to be a dominant effect. To prove this, we run Monte Carlo simulations and estimate the relative fraction of clusters that would suffer projection contamination. For simplicity, we consider only clusters with masses $10^{14}\,{\rm M}_\odot$, i.e. close to the $N_{500,c}/\sigma_{\rm field} = 3$ detection threshold. Given the steepness of the cluster mass function, the data sample will in fact be dominated by clusters at the low-mass limit. Moreover, more massive clusters will be more easily detected against projection effects. As contaminants, we consider clusters of the same mass whose centre is less than r_{200} away from the centre of another cluster, in projection. The number of clusters at any given z_c is given by the adopted cosmology, and their spatial distribution is assumed to be random in the volumes defined by the *Euclid* survey area and by the redshift range $\pm 3 \times 0.05(1 + z_c)$. We find that the fraction of clusters with at least one contaminant along the line of sight decreases from ∼20 per cent at low redshifts to ∼2 per cent at high redshifts. We ascribe this decrease to the decrease with redshift of the number of clusters and of the volume contained within $\pm 3 \times 0.05(1 + z_c)$.

While we have neglected the effect of cluster clustering in this simplistic estimate, other effects will in practice contribute to further reduce the estimated contamination. Clusters projected along the line of sight will in fact be distinguished by their mean redshift, which will be more accurate that the z_p estimates of individual galaxies, and by their galaxy number density profiles – a contaminating cluster will typically appear as an overdensity at large radii from the main density peak of the contaminated cluster.

A more quantitative assessment of the impact of projection effects requires a detailed analysis of simulated samples extracted from mocks *Euclid* surveys. While this analysis is beyond the aim of this paper, we point out that the *Euclid* collaboration will use a battery of sophisticated cluster finder algorithms to maximize the catalogue completeness and purity at any redshift.

3 FISHER MATRIX ANALYSIS

Before presenting our forecasts for the cosmological constraints we now briefly describe the FM formalism that we use to derive these constraints.

The FM formalism is a Gaussian approximation of the likelihood around the maximum to second order and it is an efficient way to study the accuracy of the estimation of a vector of parameters $\boldsymbol{p}$ by using independent data sets. The FM is defined as

$$F_{\alpha\beta} \equiv - \left\langle \frac{\partial^2 \ln \mathcal{L}}{\partial p_\alpha \partial p_\beta} \right\rangle , \quad (1)$$

where $\mathcal{L}$ is the likelihood of the observable quantity (e.g. Dodelson 2003). In our FM analysis we combine three different pieces of information: the galaxy cluster number density, the cluster PS, and the prior knowledge of cosmological parameters as derived from the *Planck* CMB experiment (Planck Collaboration XVI 2014). To quantify the constraining power of a given cosmological probe on

[2] https://code.google.com/p/idl-moustakas/source/browse/trunk/impro/cosmo/quickcv.pro?r=617

[3] http://wiki.cosmos.esa.int/euclid/index.php/EC_SGS_OU_LE3. Access restricted to members of the *Euclid* Consortium.

a pair of joint parameters (p_i, p_j) we use the figure of merit (FoM; Albrecht et al. 2006):

$$\mathrm{FoM} = \frac{1}{\sqrt{\det\left[\mathrm{Cov}\left(p_i, p_j\right)\right]}}, \tag{2}$$

where $\mathrm{Cov}(p_i, p_j)$ is the covariance matrix between the two parameters. With this definition, the FoM is proportional to the inverse of the area encompassed by the ellipse representing the 68 per cent confidence level (c.l.) for model exclusion.

As described in detail in Sartoris et al. (2010), we follow the approach of Holder, Haiman & Mohr (2001) and define the FM for the cluster NC as

$$F^N_{\alpha\beta} = \sum_{\ell,m} \frac{\partial N_{\ell,m}}{\partial p_\alpha} \frac{\partial N_{\ell,m}}{\partial p_\beta} \frac{1}{N_{\ell,m}}. \tag{3}$$

In the previous equation, the sums over ℓ and m run over redshift and mass intervals, respectively. The quantity $N_{\ell,m}$ is the number of clusters expected in a survey with a sky coverage $\Omega_{\rm sky}$, within the ℓth redshift bin and mth bin in observed mass $M^{\rm ob}$. This can be calculated as (Lima & Hu 2005)

$$N_{\ell,m} = \Delta\Omega_{\rm sky} \int_{z_\ell}^{z_{\ell+1}} \mathrm{d}z \, \frac{\mathrm{d}V}{\mathrm{d}z\,\mathrm{d}\Omega} \times \int_{M^{\rm ob}_{\ell,m}}^{M^{\rm ob}_{\ell,m+1}} \frac{\mathrm{d}M^{\rm ob}}{M^{\rm ob}} \int_0^{+\infty} \mathrm{d}M \, n(M,z) \, p(M^{\rm ob}|M), \tag{4}$$

where $\mathrm{d}V/(\mathrm{d}z\,\mathrm{d}\Omega)$ is the cosmology-dependent comoving volume element per unit redshift interval and solid angle. The lower observed mass bin is bound by $M^{\rm ob}_{\ell,m=0} = M_{\rm thr}(z)$, where $M_{\rm thr}(z)$ is defined as the threshold value of the observed mass for a cluster to be included in the survey (see Fig. 2). For the halo mass function $n(M, z)$ in equation (4), we assume the expression provided by Tinker et al. (2008). Since the *Euclid* selection function has been computed for masses at $\Delta_{\rm c} = 200$ with respect to the critical density, we use the Tinker et al. (2008) mass function parameters relevant for an overdensity of $\Delta_{\rm bk} = 200/\Omega_{\rm m}(z)$ with respect to the background density. We note that in equation (4) we have implicitly assumed that the survey sky coverage $\Omega_{\rm sky}$ is independent of the observed mass, which may not necessarily be the case if the sensitivity is not constant over the survey area. This is particularly important for the PS estimation. Currently, the *Euclid* sensitivity maps for the photometric and spectroscopic surveys have still to be fully characterized. We point out that their precise definition is of vital importance for all the cosmological probes to be carried out by *Euclid*.

In equation (4), $p(M^{\rm ob}|M)$ is the probability to assign an observed mass $M^{\rm ob}$ to a galaxy cluster with true mass M. Following Lima & Hu (2005), we use a lognormal probability density, namely

$$p(M^{\rm ob}|M) = \frac{\exp[-x^2(M^{\rm ob})]}{\sqrt{2\pi\sigma^2_{\ln M}}}, \tag{5}$$

where

$$x(M^{\rm ob}) = \frac{\ln M^{\rm ob} - \ln M_{\rm bias} - \ln M}{\sqrt{2\sigma^2_{\ln M}}}. \tag{6}$$

In the above equation $\ln M_{\rm bias}$ is the bias in the mass estimation, which encodes any scaling relation between observable and true mass and should not be confused with the bias in the galaxy distribution. $\sigma_{\ln M}$ is the intrinsic scatter in the relation between true and observed mass (see Section 4). By inserting equation (5) into equation (4), we obtain the expression for the cluster NC within a given mass and redshift bin:

$$N_{\ell,m} = \frac{\Delta\Omega_{\rm sky}}{2} \int_{z_\ell}^{z_{\ell+1}} \mathrm{d}z \, \frac{\mathrm{d}V}{\mathrm{d}z\,\mathrm{d}\Omega} \times \int_0^{+\infty} \mathrm{d}M \, n(M,z) \left[\mathrm{erfc}(x_m) - \mathrm{erfc}(x_{m+1})\right], \tag{7}$$

where $\mathrm{erfc}(x)$ is the complementary error function and $x_m = x(M^{\rm ob}_{l,m})$.

Note that in equation (3) we neglect the clustering contribution to the noise (i.e. cosmic variance). Cosmic variance is expected to be very small in the *Euclid* survey because of the very large volume covered. On the other hand, the number density of clusters will be large enough that also Poisson noise will be very small. Poisson noise is likely to be dominant in the high-mass regime and at high redshift. In particular, high-redshift clusters are fundamental in driving constraints on DE equation of state (EoS; see Fig. 5); in this case we expect Poisson noise to dominate the error budget. At low masses (e.g. those that will be reached with the 3σ selection function) and low redshifts, cosmic variance may give a comparable or even larger contribution to the noise (Hu & Kravtsov 2003). The estimation of cosmological constraints on different parameters might be affected in different ways by our neglecting the cosmic variance contribution to the noise.

The FM for the averaged redshift-space cluster PS within the ℓth redshift bin, the mth wavenumber bin, and the ith angular bin can be written as

$$F^P_{\alpha\beta} = \frac{1}{8\pi^2} \sum_{\ell,m,i} \frac{\partial \ln \bar{P}(\mu_i, k_m, z_\ell)}{\partial p_\alpha} \frac{\partial \ln \bar{P}(\mu_i, k_m, z_\ell)}{\partial p_\beta} \times V^{\rm eff}_{\ell,m,i} \, k_m^2 \Delta k \Delta\mu \tag{8}$$

(e.g. Feldman, Kaiser & Peacock 1994; Tegmark 1997), where the sums over ℓ, m, i run over bins in redshift, wavenumber, and cosine of the angle between $\boldsymbol{k}$ and the line-of-sight direction, respectively. The quantity $V^{\rm eff}(\mu_i, k_m, z_\ell)$ represents the effective volume accessible to the survey at redshift z_ℓ and wavenumber $\boldsymbol{k}$ (Tegmark 1997; Sartoris et al. 2010), and reads

$$V^{\rm eff}(\mu_i, k_m, z_\ell) = V_0(z_\ell) \frac{\tilde{n}(z_\ell)\bar{P}(\mu_i, k_m, z_\ell)}{1 + \tilde{n}(z_\ell)\bar{P}(\mu_i, k_m, z_\ell)}. \tag{9}$$

In the above equation, $V_0(z_\ell)$ is the total comoving volume contained in the unity redshift interval around z_ℓ, while $\tilde{n}(z_\ell)$ is the average number density of objects included in the survey at redshift z_ℓ,

$$\tilde{n}(z_\ell) = \int_0^{+\infty} \mathrm{d}M \, n(M, z_\ell) \, \mathrm{erfc}\left\{x[M_{\rm thr}(z_\ell)\right\}. \tag{10}$$

The cluster PS averaged over the redshift bin, appearing in equation (8), can be written as

$$\bar{P}(\mu_i, k_m, z_\ell) = \frac{1}{S_\ell} \int_{z_\ell}^{z_{\ell+1}} \mathrm{d}z \, \frac{\mathrm{d}V}{\mathrm{d}z} \, \tilde{n}^2(z) \, \tilde{P}(\mu_i, k_m, z), \tag{11}$$

where the normalization factor S_ℓ reads

$$S_\ell = \int_{z_\ell}^{z_{\ell+1}} \mathrm{d}z \, \frac{\mathrm{d}V}{\mathrm{d}z} \, \tilde{n}^2(z). \tag{12}$$

Sartoris et al. (2012) pointed out the importance of taking into account the contribution of cluster redshift-space distortions for constraining cosmological parameters. Following Kaiser (1987), we calculate the redshift-space cluster PS $\tilde{P}(\mu_i, k_m, z_\ell)$ in the linear regime according to

$$\tilde{P}(\mu_i, k_m, z_\ell) = \left[b_{\rm eff}(z_\ell) + f(z_\ell)\mu^2\right]^2 P_{\rm L}(k_m, z_\ell), \tag{13}$$

where the PS acquires a dependence on the cosine μ of the angle between the wave vector $\boldsymbol{k}$ and the line-of-sight direction. In the above equation, $b_{\rm eff}(z_\ell)$ is the linear bias weighted by the mass function (see equation 20 in Sartoris et al. 2010),

$$b_{\rm eff}(z_\ell) = \frac{1}{\tilde{n}(z_\ell)} \int_0^{+\infty} {\rm d}M\, n(M, z_\ell) \times {\rm erfc}\left\{x[M_{\rm thr}(z_\ell)]\right\}\, b(M, z_\ell). \quad (14)$$

The function $f(a) = {\rm dln}\, D(a)/{\rm dln}\, a$ is the logarithmic derivative of the linear growth rate of density perturbations, $D(a)$, with respect to the expansion factor a. $P_{\rm L}(k_m, z_\ell)$ is the linear matter PS in real space that we calculate using the CLASS code (Blas, Lesgourgues & Tram 2011). For the DM halo bias $b(M, z)$ we use the expression provided by Tinker et al. (2010).

Both the PS and the NC FMs (equations 3 and 8) are computed in the redshift range defined by the *Euclid* photometric selection function shown in Fig. 2, namely $0.2 \leq z \leq 2$, with redshift bins of constant width $\Delta z = 0.1$. We note that the limiting precision with which the redshift $z_{\rm c}$ of a cluster is determined in the photometric survey is given by $0.05(1 + z_{\rm c})/N_{500,{\rm c}}^{1/2}$, where $N_{500,{\rm c}}$ is the total number of galaxies assigned to the cluster. Therefore, the bin width is always larger than the largest error on redshift expected from the *Euclid* photometric survey (see Section 2). In equation (3), the observed mass range extends from the lowest mass limit determined by the photometric selection function ($M_{\rm thr}(z)$, see Fig. 2) up to $\log(M_{\rm ob}/{\rm M}_\odot) \leq 16$, with $\Delta\log(M_{\rm ob}/{\rm M}_\odot) = 0.2$. In the computation of the PS FM (equation 8), we adopt $k_{\rm max} = 0.14\,{\rm Mpc}^{-1}$ and $k_{\rm min} = 0.001\,{\rm Mpc}^{-1}$, with $\Delta\log(k\,{\rm Mpc}) = 0.1$. Finally, the cosine of the angle between $\boldsymbol{k}$ and the line-of-sight direction, μ, runs in the range $-1 \leq \mu \leq 1$ with nine equally spaced bins (see Sartoris et al. 2012).

4 COSMOLOGICAL AND NUISANCE PARAMETERS

In this section we discuss the cosmological parameters that have been included in the FM analysis in order to predict the constraining power of the *Euclid* photometric cluster survey and we describe the peculiarity of all the analysed models. As a starting point, we consider all the standard cosmological parameters for the concordance ΛCDM model, whose fiducial values are chosen by following Planck Collaboration XVI (2014): $\Omega_{\rm m} = 0.32$ for the present-day total matter density parameter, $\sigma_8 = 0.83$ for the normalization of the linear PS of density perturbations, $\Omega_{\rm b} = 0.049$ for the baryon density parameter, $H_0 = 67\,{\rm km\,s^{-1}\,Mpc^{-1}}$ for the Hubble constant, and $n_{\rm S} = 0.96$ for the primordial scalar spectral index. We also allow for a variation of the curvature parameter, whose fiducial value $\Omega_k = 0$ corresponds to spatial flatness.

4.1 Model with dynamical dark energy

In addition to the ΛCDM parameters, we also include parameters describing a dynamical evolution of the DE component. In the literature there are a number of models, characterized by different parametrization of the DE EoS evolution (e.g. Wetterich 2004). In this paper we study the parametrization originally proposed by Chevallier & Polarski (2001) and Linder (2003) and then adopted in the DETF. We label this parametrization as the CPL DE model, according to which the DE EoS can be written as

$$w(a) = w_0 + w_a(1 - a). \quad (15)$$

We use $w_0 = -1$ and $w_a = 0$ as reference values for the two model parameters. Thus, the cosmological parameter vector that we use in this first part of our FM analysis reads

$$\boldsymbol{p} = \{\Omega_{\rm m}, \sigma_8, w_0, w_a, \Omega_k, \Omega_{\rm b}, H_0, n_{\rm S}\}\,. \quad (16)$$

The constraints on the DE dynamical evolution obtained by combining *Planck* CMB data with *Wilkinson Microwave Anisotropy Probe* (*WMAP*) polarization and with LSS information (Planck Collaboration XVI 2014) are $w_0 = -1.04^{+0.72}_{-0.69}$ and $w_a \lesssim 1.3$ (95 per cent c.l.) assuming $\Omega_k = 0$. Currently, the evolution of the cluster NC alone does not constrain the DE equation of state parameters. However, Mantz et al. (2014) were able to obtain $w_0 = -1.03 \pm 0.18$ and $w_a = -0.1^{+0.6}_{-0.7}$ (assuming $\Omega_k = 0$), by using CMB power spectra (1-yr *Planck* data, SPT, ACT), SNIa, and BAO data at different redshifts (plus WMAP polarization; Planck Collaboration XVI 2014).

Despite these weak constraints on the CPL DE parametrization (Vikhlinin et al. 2009), cluster counts are powerful probes of the amplitude of the matter PS. For instance, σ_8 is constrained at the level of ∼8 per cent both with optically selected SDSS clusters (Rozo et al. 2010), and with SZ selected SPT clusters (Benson et al. 2013). Moreover, clusters help breaking the degeneracy between σ_8 and $\Omega_{\rm m}$ in CMB data sets, improving the constraints on the amplitude of the matter PS by a factor of ∼2 with respect to CMB constraints alone (Rozo et al. 2010).

4.2 Model with primordial non-Gaussianity

We extend the standard cosmological model by allowing primordial density fluctuations to follow a non-Gaussian distribution (e.g. Bartolo et al. 2004; Desjacques & Seljak 2010; Wang 2014). When this happens, the distribution of primordial fluctuations in Bardeen's gauge-invariant potential Φ cannot be fully described by a PS – commonly parametrized by a power law, $P_\Phi(\boldsymbol{k}) = Ak^{n_{\rm S}-4}$ (where $k \equiv \|\boldsymbol{k}\|$) – rather we need higher order statistics such as the bispectrum $B_\Phi(\boldsymbol{k}_1, \boldsymbol{k}_2, \boldsymbol{k}_3)$. Different models of inflation are known to produce different shapes of this bispectrum. Here we consider only the so-called *local shape*, where the bispectrum strength is maximized for *squeezed* configurations, in which one of the three momenta $\boldsymbol{k}_j$ is much smaller than the other two.

Within the local shape scenario, we adopt the commonly used way to parametrize the primordial non-Gaussianity, which allows us to write Bardeen's gauge invariant potential as the sum of a linear Gaussian term and a non-linear second-order term that encapsulates the deviation from Gaussianity (e.g. Salopek & Bond 1990; Komatsu & Spergel 2001):

$$\Phi = \Phi_{\rm G} + f_{\rm NL}\left(\Phi_{\rm G}^2 - \langle\Phi_{\rm G}^2\rangle\right), \quad (17)$$

where the free dimensionless parameter $f_{\rm NL}$ parametrizes the deviation from the standard Gaussian scenario. We stress that there is some ambiguity in the normalization of equation (17). We adopt the LSS convention (as opposed to the CMB convention; see Grossi et al. 2007; Carbone, Verde & Matarrese 2008; Pillepich, Porciani & Hahn 2010) where Φ is linearly extrapolated at $z = 0$ for defining the parameter $f_{\rm NL}$. The relation between the two normalizations is $f_{\rm NL} = D(z = \infty)(1 + z) f_{\rm NL}^{\rm CMB}/D(z = 0) \simeq 1.3\, f_{\rm NL}^{\rm CMB}$, where $D(z)$ is the linear growth factor with respect to the Einstein–de Sitter cosmology.

If the density perturbation field is non-Gaussian and has a positively (negatively) skewed distribution, the probability of forming large overdensities – and thus large collapsed structures – is enhanced (suppressed). Thus, the shape and the evolution of the mass function of DM haloes change (e.g. Matarrese, Verde & Jimenez

2000; LoVerde et al. 2008; Grossi et al. 2009). Following the prescription by LoVerde et al. (2008) one can modify the mass function $n(M, z)$ in equation (4) to take into account the non-Gaussian correction as follows:

$$n(M, z) = n^{(\mathrm{G})}(M, z)\frac{n_{\mathrm{PS}}(M, z)}{n_{\mathrm{PS}}^{(\mathrm{G})}(M, z)}. \tag{18}$$

In the previous equation, $n^{(\mathrm{G})}(M, z)$ is the mass function in the reference Gaussian model, while $n_{\mathrm{PS}}(M, z)$ and $n_{\mathrm{PS}}^{(\mathrm{G})}(M, z)$ represent the Press & Schechter (1974) mass functions in the non-Gaussian and reference Gaussian models, respectively (see the full equations in Sartoris et al. 2010).

In non-Gaussian scenarios the large-scale clustering of DM haloes also changes. This modification is quite important because it alters in a fairly unique way the spatial distribution of tracers of the cosmic structure, including galaxy clusters (Dalal et al. 2008; Matarrese & Verde 2008; Giannantonio & Porciani 2010). Specifically, the linear bias acquires an extra scale dependence due to primordial non-Gaussianity, and can be written as (Matarrese & Verde 2008)

$$b(M, z, k) = b^{(\mathrm{G})}(M, z) + \left[b^{(\mathrm{G})}(M, z) - 1\right]\delta_{\mathrm{c}}(z)\Gamma_R(k), \tag{19}$$

where $\Gamma_R(k)$ encapsulates the dependence on the scale and is given by an integral over the primordial bispectrum.

To summarize, the cosmological parameter vector in this non-Gaussian extension of the ΛCDM model is

$$\boldsymbol{p} = \{\Omega_{\mathrm{m}}, \sigma_8, w_0, w_a, \Omega_k, \Omega_{\mathrm{b}}, H_0, n_{\mathrm{S}}, f_{\mathrm{NL}}\}\,. \tag{20}$$

We assume $f_{\mathrm{NL}} = 0$ as the fiducial value of the non-Gaussian amplitude.

The level of primordial non-Gaussianity has recently been constrained to high precision thanks to *Planck* CMB data (Planck Collaboration XXIV 2014b), $-4 \lesssim f_{\mathrm{NL}} \lesssim 11$, for the case of a local bispectrum shape.[4] Bounds from galaxy cluster abundance show consistency with the Gaussian scenario, $-91 \lesssim f_{\mathrm{NL}} \lesssim 78$ (Shandera et al. 2013). Constraints from the distribution of clusters are even less stringent (Mana et al. 2013). The clustering of *Euclid* spectroscopic galaxies alone is expected to restrict the allowed non-Gaussian parameter space down to $\Delta f_{\mathrm{NL}} \sim$ a few (Carbone et al. 2008; Verde & Matarrese 2009; Fedeli et al. 2011).

4.3 Parametrize deviation from general relativity

We study another extension to the standard ΛCDM cosmology, based on deviations of the law of gravity from GR. As a matter of fact, a number of non-standard gravity models have been proposed in the literature (e.g. Hu & Sawicki 2007; Capozziello & de Laurentis 2011; Amendola et al. 2013) in order to explain the low-redshift accelerated expansion of the Universe without need for the DE fluid. Many of these models give rise to modifications of the late-time linear growth of cosmological structure, which can be parametrized as

$$\frac{\mathrm{d}\ln D(a)}{\mathrm{d}\ln a} = \Omega_{\mathrm{m}}^{\gamma}(a), \tag{21}$$

where γ is dubbed the *growth index* (e.g. Lahav et al. 1991). GR predicts a nearly constant and scale-independent value of $\gamma \simeq 0.55$ (e.g. Linder 2005). Significant deviations from this value would hence signal a violation of the standard theory of gravity on large scales. The corresponding vector of cosmological parameters in this case reads

$$\boldsymbol{p} = \{\Omega_{\mathrm{m}}, \sigma_8, w_0, w_a, \Omega_k, \Omega_{\mathrm{b}}, H_0, n_{\mathrm{S}}, \gamma\}\,, \tag{22}$$

with $\gamma = 0.55$ taken as our reference value. Using NC of X-ray clusters alone, Mantz et al. (2015) have found values of γ consistent with GR ($\gamma = 0.48 \pm 0.19$). From a sample of SZ-selected clusters in SPT survey $\gamma = 0.73 \pm 0.28$ has been found (Bocquet et al. 2015). While we use γ to parametrize deviations from GR, this cannot be fully inclusive of all modifications implied by non-standard gravity, e.g. spherical collapse and mass function (Kopp et al. 2013; Lombriser et al. 2013). Moreover, the γ parameter alone does not allow to consider scale-dependences of the growth factor, which for example exist in $f(R)$ theories (Pogosian & Silvestri 2008). As such, a deviation of γ from the GR reference value of 0.55 in any test of structure growth would not be easily translated into a constraint on a specific model of modified gravity.

4.4 Model with non-minimal neutrino mass

In our analysis we also consider the case of massive neutrinos, with the associated density parameter Ω_ν as the relevant parameter to be constrained. Ω_ν is related to the total neutrino mass, $\sum_i^{N_\nu} m_{\nu,i}$, through the relation

$$\Omega_\nu = \frac{\rho_\nu}{\rho_{\mathrm{c}}} = \frac{\sum_i^{N_\nu} m_{\nu,i}}{93.14\,\mathrm{h^2\,eV}}, \tag{23}$$

where ρ_ν and ρ_{c} are the $z = 0$ neutrino and critical mass densities, respectively, and N_ν is the number of massive neutrinos. A larger value of Ω_ν acts on the observed matter PS in two ways (e.g. Lesgourgues & Pastor 2006; Marulli et al. 2011; Massara, Villaescusa-Navarro & Viel 2014). The peak of the PS is shifted to larger scale, because a larger value of the radiation density postpones the time of equality. Moreover, since neutrinos free-stream over the scale of galaxy clusters, they do not contribute to the clustered collapsed mass on such a scale. As a consequence, the halo mass function at fixed value of Ω_{m} will be below the one expected in a purely CDM model. Brandbyge et al. (2010) have shown that results from *N*-body simulations with massive neutrinos can be reproduced in a more accurate way by using the Tinker et al. (2008) halo mass function with

$$\rho_{\mathrm{m}} \rightarrow \rho_{\mathrm{CDM}} + \rho_{\mathrm{b}} = \rho_{\mathrm{m}} - \rho_\nu, \tag{24}$$

where ρ_{m}, ρ_{CDM}, ρ_{b}, and ρ_ν are the total mass, CDM, baryon, and neutrino densities. Based on the analysis of an extended set of *N*-body simulations, Castorina et al. (2014) and Costanzi et al. (2013b) have shown that, since neutrinos play a negligible role in the gravitational collapse, only the contribution of cold dark matter and baryons to the PS has to be used to compute the rms of the linear matter perturbations, $\sigma(R)$, in the computation of the halo mass function and linear bias:

$$P_{\mathrm{m}} \rightarrow P_{\mathrm{CDM}}(k) = P_{\mathrm{m}}(k)\left[\frac{\Omega_{\mathrm{CDM}}T_{\mathrm{CDM}}(k, z) + \Omega_{\mathrm{b}}T_{\mathrm{b}}(k, z)}{(\Omega_{\mathrm{b}} + \Omega_{\mathrm{CDM}})T_{\mathrm{m}}(k, z)}\right]^2. \tag{25}$$

Here T_{CDM}, T_{b}, and T_{m} are the CDM, baryon, and total matter transfer functions, respectively, and P_{m} is the total matter PS.

Hence, the cosmological parameter vector we use in this case is

$$\boldsymbol{p} = \{\Omega_{\mathrm{m}}, \sigma_8, w_0, w_a, \Omega_k, \Omega_{\mathrm{b}}, H_0, n_{\mathrm{S}}, \Omega_\nu\}\,, \tag{26}$$

[4] The *Planck* CMB constraints on primordial non-Gaussianity have been converted here into the LSS convention.

with a fiducial value of $\Omega_\nu = 0.0016$ that corresponds to $\sum m_\nu = 0.06$ for three degenerate neutrinos (Carbone et al. 2012; Mantz et al. 2015). Currently, great attention has been devoted to derive constraints on the neutrino mass from the combination of galaxy clusters with other LSS observables. The analysis of the *Planck* SZ cluster sample resulted in $\sum m_\nu = 0.20 \pm 0.09$ eV (Planck Collaboration XX 2014a). Mantz et al. (2014), combining cluster, CMB, SN1a, and BAO data, found $\sum m_\nu < 0.38$ eV at 95.4 per cent c.l. in a wCDM Universe. Costanzi et al. (2014) found $\sum m_\nu < 0.15$ eV (68 per cent c.l.) in a ΛCDM Universe, for a three active neutrino scenario, using cluster counts, CMB, BAO, Lyman α, and cosmic shear data. In Bocquet et al. (2015) the analysis of SPT cluster sample resulted in $\sum m_\nu = 0.148 \pm 0.081$ eV.

4.5 Parameters of the mass–observable scaling relation

In our FM analysis, besides the cosmological parameter vectors detailed above, we also include four extra parameters to model intrinsic scatter and bias in the scaling relation between the observed and true galaxy cluster masses (see equation 6 above). We assume the following parametrization for the bias and the scatter, respectively,

$$\ln M_{\rm bias}(z) = B_{M,0} + \alpha \ln(1+z)$$

and

$$\sigma^2_{\ln M}(z) = \sigma^2_{\ln M,0} - 1 + (1+z)^{2\beta}. \quad (27)$$

We select the following fiducial values:

$$\boldsymbol{p}_{\rm nuisance,\,F} = \left\{B_{M,0} = 0, \alpha = 0, \sigma_{\ln M,0} = 0.2, \beta = 0.125\right\}. \quad (28)$$

We refer to these four parameters as *nuisance* parameters henceforth. With the fiducial nuisance parameter vector there is no bias in the true mass–observable relation and the value of the scatter at $z = 0$ is in accordance with Rykoff et al. (2012). Also, the fiducial value for β makes the scatter increase with redshift, reaching $\sigma_{\ln M} \simeq 0.6$ at the maximum redshift of the *Euclid* survey ($z_{\rm max} = 2$).

Our chosen parametrization for the bias and scatter (equation 27) stems from our current ignorance of the details of the mass–observable relations and their z and/or mass dependence. For lack of better knowledge we have chosen a simple power-law dependence on z. Recent analyses show in fact that a power law description of the mass–richness scaling relation, with Gaussian distributed intrinsic scatter, provides an accurate description of available data for low-redshift clusters (e.g. Andreon 2015). Clearly, the WL mass calibration from the wide and deep *Euclid* surveys will ultimately tell us whether the modelization of the mass–observable relation assumed for our forecasts need to be refined. In the *Euclid* survey it will be possible to calibrate such relation with its uncertainties thanks to the WL and spectroscopic surveys. We estimate that *Euclid* has the potential to calibrate the scaling relation to ≤15 per cent accuracy out to $z \leq 1.5$ (see Appendix B).

In the following section, we will consider the two extreme cases where we assume (i) no prior information on the nuisance parameters, and (ii) perfect knowledge of the mass–observable relation.

5 RESULTS

Here, we present the constraints on the cosmological parameter vectors introduced in the previous section, using the FM formalism. As a first result, we plot in Fig. 3 the histograms corresponding to the redshift distributions, $n(z) = \Delta z\, {\rm d}N/{\rm d}z$ (equation7), of *Euclid* photometric galaxy clusters, obtained by adopting the two selection

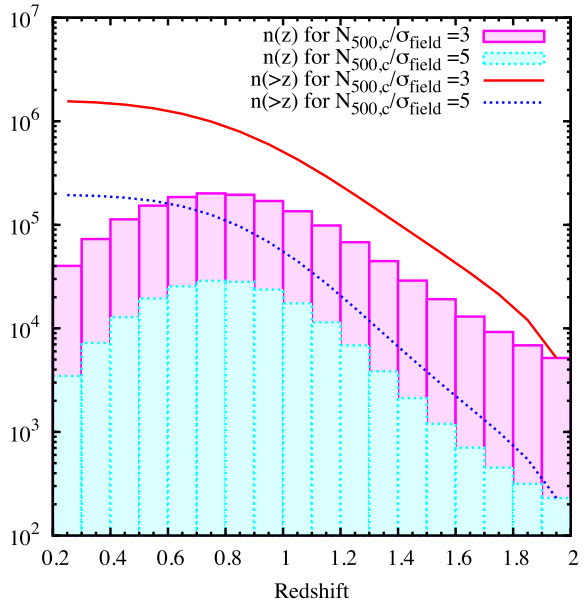

Figure 3. Number of clusters above a given redshift to be detected with overdensities $N_{500,c}/\sigma_{\rm field} > 5$ and >3 in the *Euclid* photometric survey (dotted blue and solid red lines, respectively). We also show the number density of clusters expected to be detected within redshift bins of width $\Delta z = 0.1$ for the same detection thresholds (dotted cyan and solid magenta histograms, respectively).The numbers have been obtained by using the reference values of cosmological and nuisance parameters (see Section 4).

functions, which correspond to the two different detection thresholds $N_{500,c}/\sigma_{\rm field} > 3$ and 5 (see Fig. 2), and by using the reference values of cosmological and nuisance parameters. The two curves show the corresponding cumulative redshift distributions, $n(>z)$, i.e. the total number of clusters detected above a given redshift. *Euclid* will detect ∼2 × 10^5 objects with $N_{500,c}/\sigma_{\rm field} \geq 5$ at all redshifts, with about ∼4 × 10^4 of them at $z \geq 1$. By lowering the detection threshold down to $N_{500,c}/\sigma_{\rm field} = 3$, these numbers rise up to ∼2 × 10^6 clusters at all redshifts, with ∼4 × 10^5 of them at $z \geq 1$. The large statistics of clusters at $z \geq 1$ provides a wide redshift leverage over which to follow the growth rate of perturbations. As a comparison, DES will detect ∼1.7 × 10^5 clusters (with more than 10 bright red-sequence galaxies) and with masses greater than ∼5 × 10^{13} $M_\odot$ out to $z \sim 1.5$ in the survey area of 5000 deg^2 [5] eROSITA (Pillepich, Porciani & Reiprich 2012) will detect ∼9.3 × 10^4 clusters with masses greater than ∼5 × 10^{13} $M_\odot$ in the survey area of 27 000 deg^2, almost all at $z < 1$.

In Figs 4, 6, 7, and 8 we show the forecasted constraints from *Euclid* photometric clusters on suitable pairs of cosmological parameters. The ellipses in these figures always correspond to the 68 per cent c.l. after marginalization over all other cosmological parameters and nuisance parameters. In each of these figures, the blue dotted contours are obtained by combining the NC FM (equation 3) and the cluster PS FM (equation 8), assuming no prior information on any of the cosmological and nuisance parameters. Also, the cluster sample is defined by the selection $N_{500,c}/\sigma_{\rm field} \geq 3$. The green dash–dotted contours are obtained in the same way except for the addition of strong priors on the nuisance parameters, i.e. assuming perfect knowledge of the scaling relation between the true and the observed cluster mass (this is labelled as '+known

[5] https://www.darkenergysurvey.org/reports/proposal-standalone.pdf

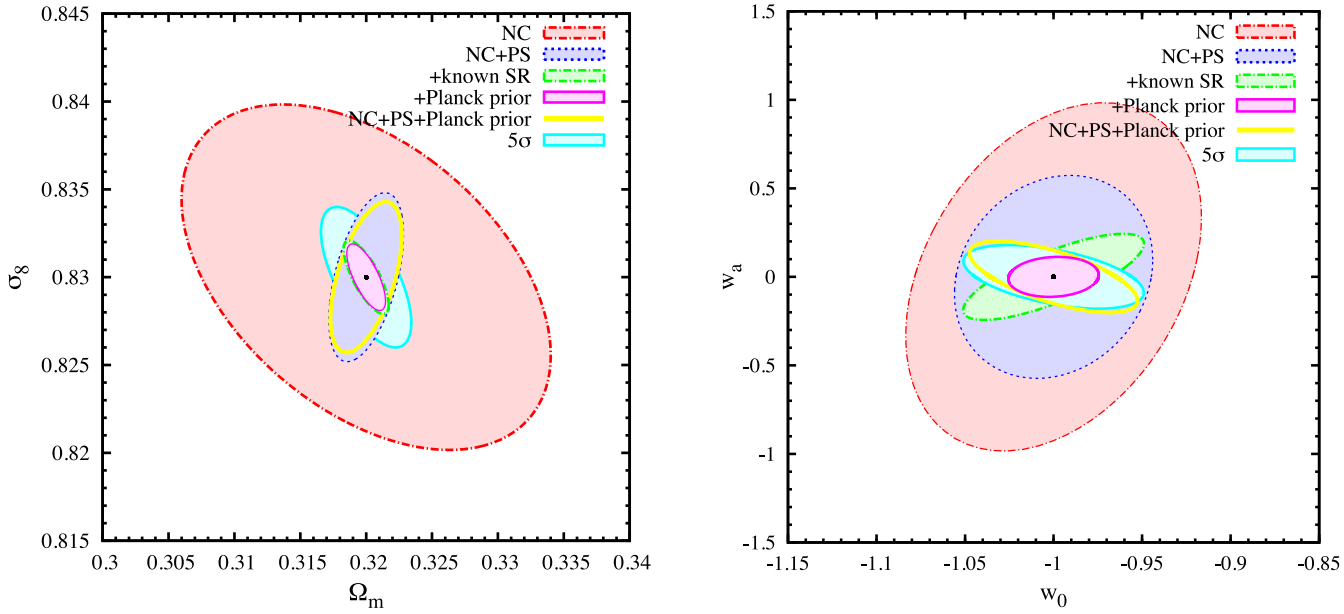

Figure 4. Constraints at the 68 per cent c.l. on the parameters $\Omega_{\rm m}$ and σ_8 (left-hand panel) and on the parameters w_0 and w_a for the DE EoS evolution (right-hand panel). In each panel, we show forecasts for the $N_{500,{\rm c}}/\sigma_{\rm field} \geq 3$ *Euclid* photometric cluster selection obtained by (i) NC, the FM NC (red dash–dotted contours), (ii) NC+PS, the combination of FM NC and PS information (blue dotted contours), (iii) NC+PS+known SR, i.e. by additionally assuming a perfect knowledge of the nuisance parameters (green dash–dotted contours), and (iv) NC+PS+known SR+*Planck* prior, i.e. by also adding information from *Planck* CMB data (magenta solid contours). With yellow solid curve we show results from the $N_{500,{\rm c}}/\sigma_{\rm field} \geq 3$ sample in the case NC+PS+*Planck* prior, i.e. with no assumption on the nuisance parameters. With cyan solid lines we show forecasts for the $N_{500,{\rm c}}/\sigma_{\rm field} \geq 5$ *Euclid* photometric cluster selection in the case NC+PS+known SR+*Planck* prior (labelled 5σ). *Planck* information includes prior on ΛCDM parameters and the DE EoS parameters.

SR' in the figures). The magenta solid contours have been obtained by further introducing prior information from *Planck* data (labelled '+*Planck* prior' in the figures). The cyan solid contours represent the same combination of information as the magenta solid ones (NC+PS+known SR+*Planck* prior) obtained from the cluster sample with selection corresponding to $N_{500,{\rm c}}/\sigma_{\rm field} \geq 5$. In the figures, we indicate these contours with the label 5σ. Finally, for the cluster sample from the selection $N_{500,{\rm c}}/\sigma_{\rm field} \geq 3$, we show, with a yellow solid curve, the constraints obtained by combining the cluster NC and PS FM, assuming no prior information on nuisance parameters, while including prior information from *Planck* data.

When using the *Planck* priors, we take for the CPL DE model the correlation matrix obtained by combining *Planck* CMB data with the BAOs from Planck Collaboration XVI (2014)[6] for the parameters of the ΛCDM cosmology (assuming $\Omega_k = 0$), plus w_0 and w_a.[7] For the non-Gaussian case, we use priors from the *Planck* obtained for the ΛCDM model plus $\Omega_{k,0}$ parameters.[8] We also added a flat prior on the level of non-Gaussianity corresponding to $-5.8 \leq f_{\rm NL}^{\rm CMB} \leq 5.8$. Finally, for the modified gravity and the neutrino scenario we also used priors from the *Planck* analysis carried out over the parameters of the ΛCDM model plus Ω_k.

In Fig. 4, we show the constraints on $\Omega_{\rm m}$ and σ_8 (left-hand panel), as well as those on the two CPL DE parameters w_0 and w_a (right-hand panel). The contours on the $\Omega_{\rm m}$–σ_8 plane for the combination of NC and clustering of $N_{500,{\rm c}}/\sigma_{\rm field} \geq 3$ galaxy clusters are rather tight. The information provided by the number density of clusters alone defines the degeneracy direction between $\Omega_{\rm m}$ and σ_8, with the following constraints: $\Delta\Omega_{\rm m} = 0.009$, $\Delta\sigma_8 = 0.006$. Information from the cluster PS alone does not provide stringent constraints on the $\Omega_{\rm m}$–σ_8 plane. However, using the combination of the PS with NC FM, the values of both parameters are constrained to high accuracy: $\Delta\Omega_{\rm m} = 0.0019$, $\Delta\sigma_8 = 0.0032$ (see Table 1). By assuming a perfect knowledge of the scaling relation between true and observed cluster mass, the bounds improve significantly. This is especially true for σ_8, which is more affected by the nuisance parameters than $\Omega_{\rm m}$. Including information from the *Planck* priors does not improve the forecasted constraints significantly.

Taking the ΛCDM as a reference model, its parameters will be constrained with a precision of $\sim 10^{-3}$,

$$\Delta\Omega_{\rm m} = 5.9 \times 10^{-4},\ \Delta\sigma_8 = 4.9 \times 10^{-4},\ \Delta h = 7.2 \times 10^{-4},$$
$$\Delta\Omega_{\rm b} = 8.4 \times 10^{-4},\ \Delta n_{\rm s} = 3.3 \times 10^{-3}, \qquad (29)$$

thanks to the unprecedented number of clusters that will be detected at high redshift. These constraints have been obtained with the $N_{500,{\rm c}}/\sigma_{\rm field} \geq 3$ selection function, from cluster NC and PS, by assuming *strong prior* on the nuisance parameters, and no prior from *Planck*.

These results emphasize the importance of exploring the high-redshift clusters in survey mode. Of course a good knowledge of the astrophysical process taking place in clusters is fundamental to calibrate the mass–observable scaling relations, and also to optimize the detection algorithms. Hence detailed follow-ups of restricted samples of clusters (such as e.g. CLASH, CCCP, WtG; Hoekstra et al. 2012; Postman et al. 2012; Rosati et al. 2014; von der Linden et al. 2014) retain a crucial importance.

On the other hand, the inclusion of *Planck* priors shall bring a substantial improvement over the bounds to the DE parameters. This result is expected, since the CMB data provide stringent constraints on the curvature, thereby breaking the degeneracy between Ω_k and

[6] Available at http://wiki.cosmos.esa.int/planckpla/index.php/Cosmological_Parameters
[7] PLA/base_w_wa/planck_lowl_lowLike_BAO
[8] PLA/base_omegak/planck_lowl_lowLike

Table 1. FoM and constraints on cosmological parameters as obtained by progressively adding the FM information for different models, for two different detection thresholds ($N_{500,c}/\sigma_{field} \geq 3$ and 5). Constraints are shown at 68 per cent c.l. after marginalization over all other cosmological parameters and nuisance parameters in the arrays.

Parameter arrays:		Equations (16) and (28)				Equations (22) and (28)	Equations (20) and (28)	Equations (26) and (28)
Constraints:	FoM	Δw_0	Δw_a	$\Delta\Omega_m$	$\Delta\sigma_8$	$\Delta\gamma$	Δf_{NL}	$\Delta\Omega_v$
$N_{500,c}/\sigma_{field} \geq 3$ *Euclid* photometric cluster selection								
NC+PS	73	0.037	0.38	0.0019	0.0032	0.023	6.67	0.0015
NC+PS+known SR	291	0.034	0.16	0.0011	0.0014	0.020	6.58	0.0013
NC+PS+known SR+*Planck*	802	0.017	0.074	0.0010	0.0012	0.015	4.93	0.0012
NC+PS+*Planck*	322	0.031	0.13	0.0018	0.0028	0.021	4.96	0.0013
$N_{500,c}/\sigma_{field} \geq 5$ *Euclid* photometric cluster selection								
NC+PS+known SR+*Planck*	209	0.034	0.12	0.0022	0.0026	0.034	6.74	0.0020
NC+PS+*Planck*	94	0.080	0.32	0.0030	0.0064	0.051	6.78	0.0027

the evolution of the DE EoS (Sartoris et al. 2012). The contribution of the PS information is less important for (w_0, w_a) with respect to (Ω_m, σ_8); however, the FoM increases from ∼30 in the case of NC alone to ∼73 for NC+PS constraints (see Table 1). For both DE EoS parameters, it is crucial to have a well-calibrated scaling relation over the redshift range sampled by the cluster survey (Sartoris et al. 2012). Indeed, by combining NC and PS, and assuming perfect knowledge of the scaling relation increases the FoM to ≃291. When we also include the *Planck* data, i.e. we set a prior on the curvature, we obtain FoM = 802, with $\Delta w_0 = 0.017$ and $\Delta w_a = 0.07$. Moreover when we add the *Planck* data to NC and PS information without assuming any knowledge on the nuisance parameters, we obtain FoM = 322, with $\Delta w_0 = 0.031$ and $\Delta w_a = 0.13$ (see Table 1). We point out that only in this analyse where we study the CPL model, we use the *Planck* CMB data combined with the BAOs information as provided by Planck Collaboration XVI (2014).

When we restrict our analysis to the wCDM model (that is characterized by the six free parameters $\Omega_m, \sigma_8, h, \Omega_b, n_s, w$), we obtain $\Delta w = 0.005$. If we also add w_a as a free parameter, we obtain $\Delta w_0 = 0.013$ and $\Delta w_a = 0.048$. These constraints have been obtained with the $N_{500,c}/\sigma_{field} \geq 3$ selection function, from cluster NC and PS, by assuming *strong prior* on the nuisance parameters, and no prior from *Planck*.

In both panels of Fig. 4, the adoption of a more conservative cluster selection ($N_{500,c}/\sigma_{field} \geq 5$) significantly worsens the forecasted cosmological constraints. For instance, the FoM is degraded down to 209 in the best-case scenario, as a consequence of the significantly degraded statistics corresponding to the higher selection threshold.

In Fig. 5, we show how the FoM depends on the limiting redshift of the survey. The FoM shown in this figure refers to NC in the $N_{500,c}/\sigma_{field} \geq 3$ *Euclid* photometric cluster selection. The FoM for a survey reaching out to $z \leq 1.2$ is only half the FoM of an equivalent survey reaching out to $z \leq 2$. It is therefore important that the redshift range covered by the survey be large enough to allow a comparison of the behaviour of DE over a sufficiently long cosmological time-scale. In this sense, the *Euclid* survey will have a unique advantage over other existing and planned surveys.

In Fig. 6, we show cosmological constraints in the expanded parameter space which includes non-Gaussian primordial density fluctuations. Specifically, we display the constraints in the f_{NL}–σ_8 plane. Thanks to the peculiar scale dependence that primordial non-Gaussianity induces on the linear bias parameter, the PS of the cluster distribution turns out to be much more sensitive to f_{NL} than it is to σ_8. This is clearly demonstrated by the red dash–dotted contour, which shows forecasted constraints derived from cluster clustering alone. Quite clearly, σ_8 is basically unconstrained on the scale of the

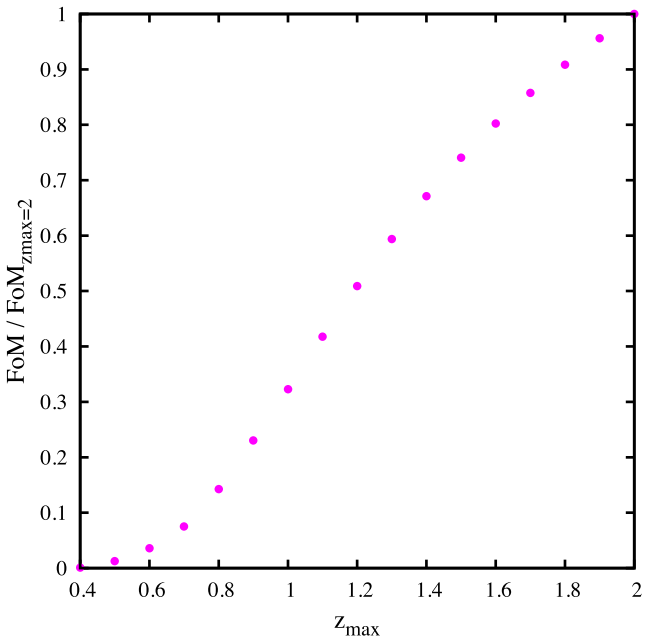

Figure 5. Relative FoM for NC in the $N_{500,c}/\sigma_{field} \geq 3$ *Euclid* photometric cluster selection, as a function of the limiting redshift z_{max} of the survey, i.e. the ratio between the FoM evaluated over $0.2 \leq z \leq z_{max}$ and the FoM evaluated over $0.2 \leq z \leq 2.0$.

figure, while f_{NL} is constrained with an uncertainty $\Delta f_{NL} \sim 7.4$. The addition of cluster NC changes very little the bounds for primordial non-Gaussianity, however, it improves substantially those for the amplitude of the matter PS (see Table 1). This helps to define the degeneracy between f_{NL} and σ_8 that are both related to the timing of structure formation. Interestingly, the estimation of primordial non-Gaussianity is weakly sensitive to the nuisance parameters. Indeed, when a perfect knowledge of the scaling relation between true and observed cluster mass is assumed, only the constraints on σ_8 improve significantly. *Planck* priors does not affect substantially the constraints on f_{NL}.

When we restrict our analysis to the ΛCDM model plus the non-Gaussianity parameter f_{NL}, we obtain $\Delta f_{NL} = 6.44$. This constraint has been obtained with the $N_{500,c}/\sigma_{field} \geq 3$ selection function, from cluster NC and PS, by assuming *strong prior* on the nuisance parameters, and no prior from *Planck*. Forecast for eROSITA (Pillepich et al. 2012) predict a similar precision, since the narrower redshift range of this survey (with respect to *Euclid*) is compensated by its wider area, which allows a better sampling of large-scale modes.

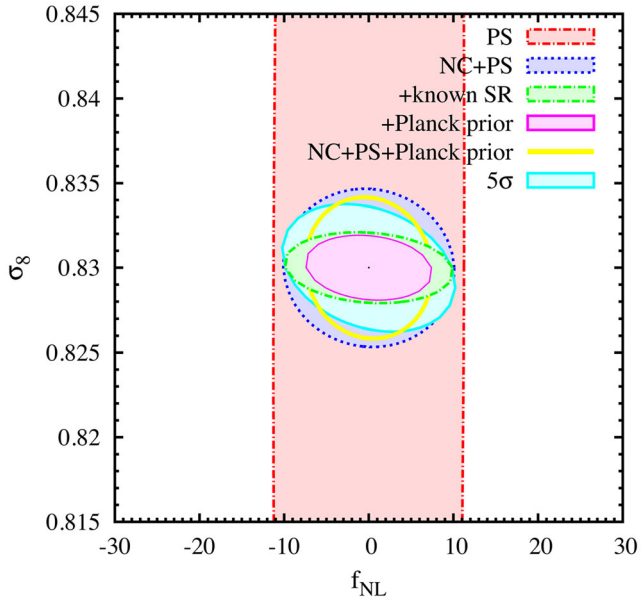

Figure 6. Constraints at the 68 per cent c.l. on the $f_{\rm NL}$–σ_8 parameters. We show forecasts for the $N_{500,c}/\sigma_{\rm field} \geq 3$ *Euclid* photometric cluster selection obtained by (i) PS, the FM PS (red dash–dotted contours), (ii) NC+PS, the combination of FM NC and PS information (blue dotted contours), (iii) NC+PS+known SR, i.e. by additionally assuming a perfect knowledge of the nuisance parameters (green dash–dotted contours), and (iv) NC+PS+known SR+*Planck* prior, i.e. by also adding information from *Planck* CMB data (magenta solid contours). With yellow solid curve we show results from the $N_{500,c}/\sigma_{\rm field} \geq 3$ sample in the case NC+PS+*Planck* prior, i.e. with no assumption on the nuisance parameters. With cyan solid lines we show forecasts for the $N_{500,c}/\sigma_{\rm field} \geq 5$ *Euclid* photometric cluster selection in the case NC+PS+known SR+*Planck* prior (labelled 5σ). *Planck* information includes prior on ΛCDM+Ω_k+$f_{\rm NL}$ parameters.

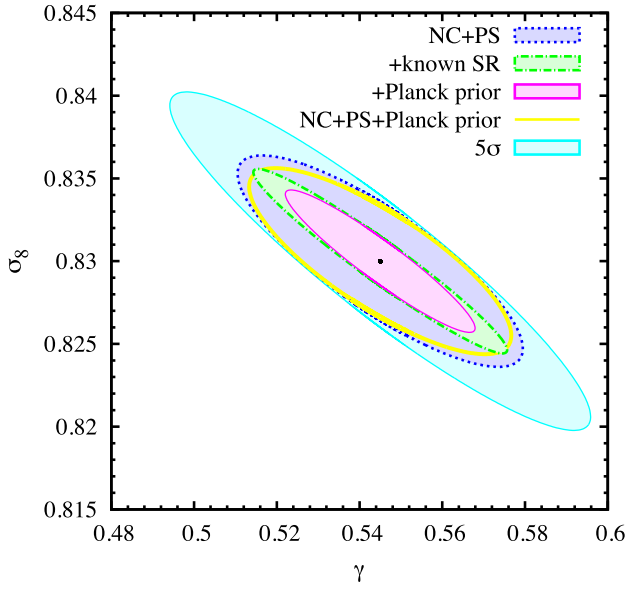

Figure 7. Constraints at the 68 per cent c.l. on the γ–σ_8 parameter plane. We show forecasts for the $N_{500,c}/\sigma_{\rm field} \geq 3$ *Euclid* photometric cluster selection obtained by (i) NC+PS, the combination of FM NC and PS information (blue dotted contours), (ii) NC+PS+known SR, i.e. by additionally assuming a perfect knowledge of the nuisance parameters (green dash–dotted contours), and (iii) NC+PS+known SR+*Planck* prior, i.e. by also adding information from *Planck* CMB data (magenta solid contours). With yellow solid curve we show results from the $N_{500,c}/\sigma_{\rm field} \geq 3$ sample in the case NC+PS+*Planck* prior, i.e. with no assumption on the nuisance parameters. With cyan solid lines we show forecasts for the $N_{500,c}/\sigma_{\rm field} \geq 5$ *Euclid* photometric cluster selection in the case NC+PS+known SR+*Planck* prior (labelled 5σ). *Planck* information includes prior on ΛCDM+Ω_k parameters.

We point out that in this analysis we are assuming the most commonly used parametrization of non-Gaussianity, where $f_{\rm NL}$ is considered scale invariant. However, there are models that predict otherwise. For these, the combination of clusters and CMB data complement each other well, providing tight constraints on the possible scale dependence of $f_{\rm NL}$.

As for the models including GR violation, we show in Fig. 7 the constraints on σ_8 and the growth parameter γ. Similarly to the constraints on the $\Omega_{\rm m}$–σ_8 plane, the constraints on γ are not strongly affected by the inclusion of *Planck* priors, thus implying that galaxy clusters are by themselves excellent tools to detect signature of modified gravity through its effect on the growth of perturbations. Significant degradation of the constraining power happens if a higher threshold for cluster detection is chosen.

Restricting our analysis to the ΛCDM model plus the γ parameter we obtain $\Delta\gamma = 0.006$. This constraint has been obtained with the $N_{500,c}/\sigma_{\rm field} \geq 3$ selection function, from cluster NC and PS, by assuming *strong prior* on the nuisance parameters, and no prior from *Planck*.

Finally, we show in Fig. 8 the joint cosmological constraints on σ_8 and the neutrino density parameter Ω_ν. The presence of neutrinos with masses in the sub-eV range requires higher values of σ_8: increasing Ω_ν at fixed $\Omega_{\rm m}$ has the effect of shifting the epoch of matter-radiation equality to a later time and to reduce the growth of density perturbations at small scales in the post-recombination epoch. As a consequence, a larger value of σ_8 is required to compensate these effects. We use the *Planck* prior mainly to add information

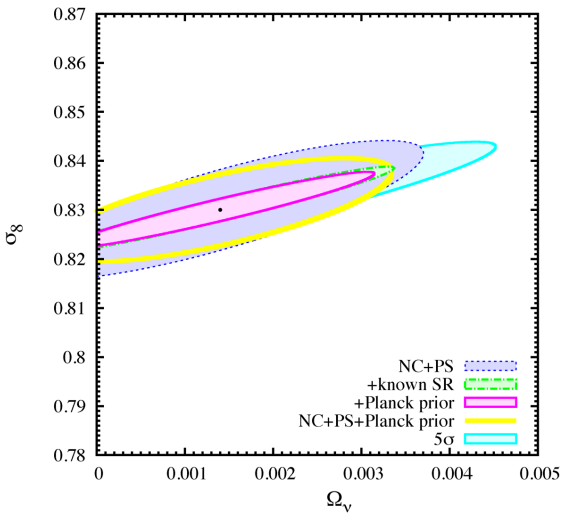

Figure 8. Constraints at the 68 per cent c.l. in the Ω_ν–σ_8 parameter plane. We show forecasts for the $N_{500,c}/\sigma_{\rm field} \geq 3$ *Euclid* photometric cluster selection obtained by (i) NC+PS, the combination of FM NC and PS information (blue dotted contours), (ii) NC+PS+known SR, i.e. by additionally assuming a perfect knowledge of the nuisance parameters (green dash–dotted contours), and (iii) NC+PS+known SR+*Planck* prior, i.e. by also adding information from *Planck* CMB data (magenta solid contours). With yellow solid curve we show results from the $N_{500,c}/\sigma_{\rm field} \geq 3$ sample in the case NC+PS+*Planck* prior, i.e. with no assumption on the nuisance parameters. With cyan solid lines we show forecasts for the $N_{500,c}/\sigma_{\rm field} \geq 5$ *Euclid* photometric cluster selection in the case NC+PS+known SR+*Planck* prior (labelled 5σ). *Planck* information includes prior on ΛCDM+Ω_k parameters.

on the geometry of the Universe, and the standard ΛCDM parameters. We obtain the constraints $\Delta\Omega_\nu = 0.0012$ (corresponding to $\Delta\sum m_\nu = 0.01$). The constraints on the neutrino density parameter are weakly affected by the inclusion of a prior on the nuisance parameters. However, there is a degradation by a factor of ∼2 of the constraining power if the selection function with the higher threshold for cluster detection is chosen (see Table 1).

To gauge the impact of a particular choice of the selection function on the cosmological constraints, we have so far shown our results for both the $N_{500,c}/\sigma_{\rm field} \geq 3$ and the $N_{500,c}/\sigma_{\rm field} \geq 5$ *Euclid* photometric cluster selection functions. As a further test, we consider the effect on the (w_0, w_a) constraints of adopting a flat selection function with $\log(M_{200,c}) = 13.9$, within $0.2 \leq z \leq 2$. With this *flat* selection function there are less clusters than with the $N_{500,c}/\sigma_{\rm field} \geq 3$ one, both in total (∼1.4×10^6 versus ∼1.6×10^6, respectively) and within $0.4 \lesssim z \lesssim 1.2$. However, the number of clusters at $z > 1$ is higher (∼3.2×10^5) for the *flat* selection function than for the $N_{500,c}/\sigma_{\rm field} \geq 3$ one (∼1.9×10^5). The effect of a larger number of high-z clusters in the *flat* selection function sample compensates for the smaller total number of clusters in providing similar constraints on the cosmological parameters to those obtained with the $N_{500,c}/\sigma_{\rm field} \geq 3$ selection function sample (changes are <10 per cent on the constraints on the DE parameters). This suggests that the precise shape of the selection function has little impact on our results, and in any case much less than its overall normalization.

6 CONCLUSIONS

In this paper, we presented a comprehensive analysis of the forecasts on the parameters that describe different extensions of the standard ΛCDM model. These were based on the selection function of galaxy clusters from the wide photometric survey to be carried out with the *Euclid* satellite, a medium-size ESA mission to be launched in 2020. We presented the derivation of this selection function and the FM formalism employed to derive cosmological constraints. This is the same formalism that has been used in the *Euclid Red Book* (Laureijs et al. 2011). Our main results can be summarized as follows.

(i) Using photometric selection, we found that *Euclid* will detect galaxy clusters at $N_{500,c}/\sigma_{\rm field} \geq 3$ with a minimum mass of ∼0.9–1 × $10^{14}\,{\rm M}_\odot$. As a result, the *Euclid* photometric cluster catalogue should include ∼2×10^6 objects, with about one-fifth of them at $z \geq 1$.

(ii) The *Euclid* cluster catalogue has the potential of providing tight constraints on a number of cosmological parameters, such as the normalization of the matter PS σ_8, the total matter density parameter $\Omega_{\rm m}$, a redshift-dependent DE equation of state, primordial non-Gaussianity, modified gravity, and neutrino masses (see Table 1). We predict that most of these constraints will be even tighter than current bounds available from *Planck*. The constraining power of the *Euclid* cluster catalogue relies on its unique broad redshift coverage, reaching out to $z = 2$.

(iii) Knowledge of the scaling relation between the true and the observed cluster mass turns out to be one of the most important factors determining the constraining power of the *Euclid* cluster catalogue for cosmology. The *Euclid* mission will have a distinct advantage in this respect, namely the possibility to calibrate such relation, at least up to $z = 1.5$, with $\lesssim$10 and $\lesssim$30 per cent accuracy, using the WL and spectroscopic surveys, respectively (see Appendix B). The deep *Euclid* survey will allow to extend the calibration to even higher redshifts, although with lower precision than in the wide survey, due to lower number statistics.

The main goal of this paper is to show how we can extract the information from clusters in the *Euclid* survey to optimally measure the cosmological parameters in various models. For this reason we have neglected at this stage some phenomenological aspects common to all observational surveys, e.g. contamination by projection effects and the non-uniform coverage of the survey. We argued that contamination is unlikely to be a dominant systematic effect in the selection function, thanks to the availability of precise photometric redshift estimates. The non-uniform coverage will be characterized with sufficient precision to allow the determination of galaxy clustering, one of the main cosmological probes of the *Euclid* survey.

With the future large surveys, like *Euclid*, that will be carried out with the next generation of telescopes, the number of detected clusters from the individual surveys will range from thousands to tens of thousands. As we have shown in this paper, this will allow to constrain most cosmological parameters to a precision level of a few per cent. Currently, theoretical halo mass functions are defined with an uncertainty of ∼5 per cent in the standard ΛCDM model (e.g. Tinker et al. 2008), and many efforts have been devoted in the last years to better sample the high-mass regime (Watson et al. 2013) and to assess the degree of universality of the halo mass function (Despali et al. 2016). To maximally extract cosmological information from these cluster surveys, it becomes critical to specify the theoretical halo mass function to better than a few per cent accuracy for a range of cosmologies. A substantial effort is currently ongoing in this direction (Grossi et al. 2007; Dalal et al. 2008; Cui, Baldi & Borgani 2012; Lombriser et al. 2013; Castorina et al. 2014). Moreover, cosmological hydrodynamic simulations will have to precise the impact of baryons on the shape of the mass profile, which has already been shown to be non-negligible (Rudd, Zentner & Kravtsov 2008; Stanek, Rudd & Evrard 2009; Cui, Borgani & Murante 2014; Cusworth et al. 2014; Martizzi et al. 2014; Velliscig et al. 2014; Vogelsberger et al. 2014; Bocquet et al. 2016; Schaller et al. 2015). While we have not addressed in this paper the impact of uncertainties in the calibration of the halo mass function and of the mass-dependent bias, it is clear that these represent theoretical uncertainties that need to be controlled at the level of few per cent if we want to take full advantage of unique characteristics of the *Euclid* cluster survey (Balaguera-Antolínez & Porciani 2013).

ACKNOWLEDGEMENTS

We thank L. Pozzetti for providing us with her estimates of the number densities of Hα emitting galaxies in advance of publication. We acknowledge useful discussions with O. Cucciati, S. Farrens, A. Iovino, S. Mei, and F. Villaescusa. We thank S. Andreon, M. Brodwin, G. De Lucia, S. Ettori, M. Girardi, T. Kitching, G. Mamon, J. Mohr, and T. Reiprich for a careful reading of the manuscript. BS acknowledges financial support from MIUR PRIN2010-2011 (J91J12000450001) and a grant from 'Consorzio per la Fisica – Trieste'. BS and SB acknowledge financial support from the PRIN-MIUR 201278X4FL grant, from a PRIN-INAF/2012 Grant, from the 'InDark' INFN Grant and from the 'Consorzio per la Fisica di Trieste'. BA acknowledges received funding from the European Union's Horizon 2020 research and innovation programme under the Marie Sklodowska-Curie grant agreement no. 656354. CF has received funding from the European Commission Seventh Framework Programme (FP7/2007-2013) under grant

agreement no. 267251. CG acknowledges CNES for financial support. LM acknowledges financial contributions from contracts ASI/INAF n.I/023/12/0. JW acknowledges support from the Transregional Collaborative Research Centre TRR 33 – 'The Dark Universe'. The authors acknowledge the *Euclid* Collaboration, the European Space Agency, and the support of a number of agencies and institutes that have supported the development of *Euclid*.

A detailed complete list is available on the *Euclid* web site (http://www.euclid-ec.org). In particular the Agenzia Spaziale Italiana, the Centre National d'Études Spatiales, the Deutches Zentrum fur Luft- and Raumfahrt, the Danish Space Research Institute, the Fundação para a Ciênca e a Tecnologia, the Ministerio de Economia y Competitividad, the National Aeronautics and Space Administration, the Netherlandse Onderzoekschool Voor Astronomie, the Norvegian Space Center, the Romanian Space Agency, the United Kingdom Space Agency, and the University of Helsinki.

REFERENCES

Abell G. O., Corwin H. G., Jr, Olowin R. P., 1989, ApJS, 70, 1
Albrecht A. et al., 2006, preprint (arXiv:astro-ph/0609591)
Albrecht A. et al., 2009, preprint (arXiv:0901.0721)
Allen S. W., Evrard A. E., Mantz A. B., 2011, ARA&A, 49, 409
Amendola L. et al., 2013, Living Rev. Relativ., 16, 6
Anderson L. et al., 2014, MNRAS, 441, 24
Andreon S., 2015, A&A, 582, A100
Andreon S., Congdon P., 2014, A&A, 568, A23
Andreon S., Hurn M. A., 2012, preprint (arXiv:1210.6232)
Arnaud M., Pratt G. W., Piffaretti R., Böhringer H., Croston J. H., Pointecouteau E., 2010, A&A, 517, A92
Balaguera-Antolínez A., Porciani C., 2013, J. Cosmol. Astropart. Phys., 4, 022
Balogh M. L., Couch W. J., Smail I., Bower R. G., Glazebrook K., 2002, MNRAS, 335, 10
Bartolo N., Komatsu E., Matarrese S., Riotto A., 2004, Phys. Rep., 402, 103
Basse T., Eggers Bjælde O., Hamann J., Hannestad S., Wong Y. Y. Y., 2014, J. Cosmol. Astropart. Phys., 5, 021
Battye R. A., Weller J., 2003, Phys. Rev. D, 68, 083506
Benson B. A. et al., 2013, ApJ, 763, 147
Betoule M. et al., 2014, A&A, 568, A22
Biviano A., Murante G., Borgani S., Diaferio A., Dolag K., Girardi M., 2006, A&A, 456, 23
Blas D., Lesgourgues J., Tram T., 2011, J. Cosmol. Astropart. Phys., 7, 34
Bocquet S. et al., 2015, ApJ, 799, 214
Bocquet S., Saro A., Dolag K., Mohr J. J., 2016, MNRAS, 456, 2361
Borgani S. et al., 2001, ApJ, 561, 13
Boselli A. et al., 1997, A&A, 324, L13
Brandbyge J., Hannestad S., Haugbølle T., Wong Y. Y. Y., 2010, J. Cosmol. Astropart. Phys., 9, 14
Brodwin M., Gonzalez A. H., Moustakas L. A., Eisenhardt P. R., Stanford S. A., Stern D., Brown M. J. I., 2007, ApJ, 671, L93
Brodwin M. et al., 2013, ApJ, 779, 138
Burenin R. A., Vikhlinin A. A., 2012, Astron. Lett., 38, 347
Capozziello S., de Laurentis M., 2011, Phys. Rep., 509, 167
Carbone C., Verde L., Matarrese S., 2008, ApJ, 684, L1
Carbone C., Fedeli C., Moscardini L., Cimatti A., 2012, J. Cosmol. Astropart. Phys., 3, 23
Carlstrom J. E. et al., 2011, PASP, 123, 568
Castorina E., Sefusatti E., Sheth R. K., Villaescusa-Navarro F., Viel M., 2014, J. Cosmol. Astropart. Phys., 2, 49
Chevallier M., Polarski D., 2001, Int. J. Modern Phys. D, 10, 213
Ciliegi P. et al., 2005, A&A, 441, 879
Clerc N., Sadibekova T., Pierre M., Pacaud F., Le Fèvre J.-P., Adami C., Altieri B., Valtchanov I., 2012, MNRAS, 423, 3561
Costanzi M., Sartoris B., Xia J.-Q., Biviano A., Borgani S., Viel M., 2013a, J. Cosmol. Astropart. Phys., 6, 20
Costanzi M., Villaescusa-Navarro F., Viel M., Xia J.-Q., Borgani S., Castorina E., Sefusatti E., 2013b, J. Cosmol. Astropart. Phys., 12, 12
Costanzi M., Sartoris B., Viel M., Borgani S., 2014, J. Cosmol. Astropart. Phys., 10, 81
Cui W., Baldi M., Borgani S., 2012, MNRAS, 424, 993
Cui W., Borgani S., Murante G., 2014, MNRAS, 441, 1769
Cusworth S. J., Kay S. T., Battye R. A., Thomas P. A., 2014, MNRAS, 439, 2485
Dalal N., Doré O., Huterer D., Shirokov A., 2008, Phys. Rev. D, 77, 123514
De Boni C., Ettori S., Dolag K., Moscardini L., 2013, MNRAS, 428, 2921
de Propris R., Eisenhardt P. R., Stanford S. A., Dickinson M., 1998, ApJ, 503, L45
Desjacques V., Seljak U., 2010, Classical Quantum Gravity, 27, 124011
Despali G., Giocoli C., Angulo R. E., Tormen G., Sheth R. K., Baso G., Moscardini L., 2016, MNRAS, 456, 2486
Dodelson S., 2003, Modern Cosmology. Academic Press, Amsterdam
Elbaz D. et al., 2007, A&A, 468, 33
Ettori S., 2013, MNRAS, 435, 1265
Fedeli C., Carbone C., Moscardini L., Cimatti A., 2011, MNRAS, 414, 1545
Feldman H. A., Kaiser N., Peacock J. A., 1994, ApJ, 426, 23
Geach J. E. et al., 2010, MNRAS, 402, 1330
Giannantonio T., Porciani C., 2010, Phys. Rev. D, 81, 063530
Giodini S., Lovisari L., Pointecouteau E., Ettori S., Reiprich T. H., Hoekstra H., 2013, Space Sci. Rev., 177, 247
Grossi M., Dolag K., Branchini E., Matarrese S., Moscardini L., 2007, MNRAS, 382, 1261
Grossi M., Verde L., Carbone C., Dolag K., Branchini E., Iannuzzi F., Matarrese S., Moscardini L., 2009, MNRAS, 398, 321
Haiman Z., Mohr J. J., Holder G. P., 2001, in Wheeler J. C., Martel H., eds, AIP Conf. Proc. Vol. 586, Relativistic Astrophysics: 20th Texas Symposium. Am. Inst. Phys., New York, p. 303
Hinshaw G. et al., 2013, ApJS, 208, 19
Hoekstra H., Mahdavi A., Babul A., Bildfell C., 2012, MNRAS, 427, 1298
Holder G., Haiman Z., Mohr J. J., 2001, ApJ, 560, L111
Hu W., Kravtsov A. V., 2003, ApJ, 584, 702
Hu W., Sawicki I., 2007, Phys. Rev. D, 76, 064004
Hütsi G., 2010, MNRAS, 401, 2477
Iglesias-Páramo J., Boselli A., Cortese L., Vílchez J. M., Gavazzi G., 2002, A&A, 384, 383
Kaiser N., 1987, MNRAS, 227, 1
Kitching T. D. et al., 2014, MNRAS, 442, 1326
Kodama T., Arimoto N., 1997, A&A, 320, 41
Kodama T., Balogh M. L., Smail I., Bower R. G., Nakata F., 2004, MNRAS, 354, 1103
Koester B. P. et al., 2007, ApJ, 660, 239
Komatsu E., Spergel D. N., 2001, Phys. Rev. D, 63, 063002
Kopp M., Appleby S. A., Achitouv I., Weller J., 2013, Phys. Rev. D, 88, 084015
Kravtsov A. V., Borgani S., 2012, ARA&A, 50, 353
Kravtsov A. V., Vikhlinin A., Nagai D., 2006, ApJ, 650, 128
Lahav O., Lilje P. B., Primack J. R., Rees M. J., 1991, MNRAS, 251, 128
Laureijs R. et al., 2011, preprint (arXiv:1110.3193)
Lesgourgues J., Pastor S., 2006, Phys. Rep., 429, 307
Lima M., Hu W., 2005, Phys. Rev. D, 72, 043006
Lin Y.-T., Mohr J. J., Stanford S. A., 2003, ApJ, 591, 749
Lin Y.-T., Mohr J. J., Gonzalez A. H., Stanford S. A., 2006, ApJ, 650, L99
Linder E. V., 2003, Phys. Rev. Lett., 90, 091301
Linder E. V., 2005, Phys. Rev. D, 72, 043529
Lombriser L., Li B., Koyama K., Zhao G.-B., 2013, Phys. Rev. D, 87, 123511
LoVerde M., Miller A., Shandera S., Verde L., 2008, J. Cosmol. Astropart. Phys., 4, 14
Mamon G. A., Biviano A., Boué G., 2013, MNRAS, 429, 3079
Mana A., Giannantonio T., Weller J., Hoyle B., Hütsi G., Sartoris B., 2013, MNRAS, 434, 684
Mancone C. L., Gonzalez A. H., Brodwin M., Stanford S. A., Eisenhardt P. R. M., Stern D., Jones C., 2010, ApJ, 720, 284
Mancone C. L. et al., 2012, ApJ, 761, 141

Mannucci F., Basile F., Poggianti B. M., Cimatti A., Daddi E., Pozzetti L., Vanzi L., 2001, MNRAS, 326, 745
Mantz A. B., Allen S. W., Morris R. G., Rapetti D. A., Applegate D. E., Kelly P. L., von der Linden A., Schmidt R. W., 2014, MNRAS, 440, 2077
Mantz A. B. et al., 2015, MNRAS, 446, 2205
Marriage T. A. et al., 2011, ApJ, 737, 61
Martizzi D., Mohammed I., Teyssier R., Moore B., 2014, MNRAS, 440, 2290
Marulli F., Carbone C., Viel M., Moscardini L., Cimatti A., 2011, MNRAS, 418, 346
Massara E., Villaescusa-Navarro F., Viel M., 2014, J. Cosmol. Astropart. Phys., 12, 053
Matarrese S., Verde L., 2008, ApJ, 677, L77
Matarrese S., Verde L., Jimenez R., 2000, ApJ, 541, 10
Mehrtens N. et al., 2012, MNRAS, 423, 1024
Merloni A. et al., 2012, preprint (arXiv:1209.3114)
Metcalfe N., Shanks T., Weilbacher P. M., McCracken H. J., Fong R., Thompson D., 2006, MNRAS, 370, 1257
Navarro J. F., Frenk C. S., White S. D. M., 1997, ApJ, 490, 493
Pillepich A., Porciani C., Hahn O., 2010, MNRAS, 402, 191
Pillepich A., Porciani C., Reiprich T. H., 2012, MNRAS, 422, 44
Planck Collaboration XI, 2011, A&A, 536, A11
Planck Collaboration XVI, 2014, A&A, 571, A16
Planck Collaboration XX, 2014a, A&A, 571, A20
Planck Collaboration XXIV, 2014b, A&A, 571, A24
Poggianti B. M., De Lucia G., Varela J., Aragon-Salamanca A., Finn R., Desai V., von der Linden A., White S. D. M., 2010, MNRAS, 405, 995
Pogosian L., Silvestri A., 2008, Phys. Rev. D, 77, 023503
Popesso P. et al., 2012, A&A, 537, A58
Postman M. et al., 2005, ApJ, 623, 721
Postman M. et al., 2012, ApJS, 199, 25
Pozzetti L. et al., 2016, A&A, in press (arXiv:1603.01453)
Press W. H., Schechter P., 1974, ApJ, 187, 425
Ramella M., Boschin W., Geller M. J., Mahdavi A., Rines K., 2004, AJ, 128, 2022
Rapetti D., Blake C., Allen S. W., Mantz A., Parkinson D., Beutler F., 2013, MNRAS, 432, 973
Reichert A., Böhringer H., Fassbender R., Mühlegger M., 2011, A&A, 535, A4
Rines K., Geller M. J., 2008, AJ, 135, 1837
Rosati P. et al., 2014, Messenger, 158, 48
Rozo E. et al., 2010, ApJ, 708, 645
Rozo E., Rykoff E., Koester B., Nord B., Wu H.-Y., Evrard A., Wechsler R., 2011, ApJ, 740, 53
Rozo E., Evrard A. E., Rykoff E. S., Bartlett J. G., 2014, MNRAS, 438, 62
Rudd D. H., Zentner A. R., Kravtsov A. V., 2008, ApJ, 672, 19
Rykoff E. S. et al., 2012, ApJ, 746, 178
Salopek D. S., Bond J. R., 1990, Phys. Rev. D, 42, 3936
Sartoris B., Borgani S., Fedeli C., Matarrese S., Moscardini L., Rosati P., Weller J., 2010, MNRAS, 407, 2339
Sartoris B., Borgani S., Rosati P., Weller J., 2012, MNRAS, 423, 2503
Schaller M. et al., 2015, MNRAS, 451, 1247
Schechter P., 1976, ApJ, 203, 297
Schuecker P., Böhringer H., Collins C. A., Guzzo L., 2003, A&A, 398, 867
Shandera S., Mantz A., Rapetti D., Allen S. W., 2013, J. Cosmol. Astropart. Phys., 8, 4
Smith G. P., Treu T., Ellis R. S., Moran S. M., Dressler A., 2005, ApJ, 620, 78
Sobral D., Best P. N., Geach J. E., Smail I., Cirasuolo M., Garn T., Dalton G. B., Kurk J., 2010, MNRAS, 404, 1551
Stanek R., Rudd D., Evrard A. E., 2009, MNRAS, 394, L11
Staniszewski Z. et al., 2009, ApJ, 701, 32
Stefanon M., Marchesini D., 2013, MNRAS, 429, 881
Sunyaev R. A., Zeldovich Y. B., 1972, Comments Astrophys. Space Phys., 4, 173
Tegmark M., 1997, Phys. Rev. Lett., 79, 3806
Tinker J., Kravtsov A. V., Klypin A., Abazajian K., Warren M., Yepes G., Gottlöber S., Holz D. E., 2008, ApJ, 688, 709
Tinker J. L., Robertson B. E., Kravtsov A. V., Klypin A., Warren M. S., Yepes G., Gottlöber S., 2010, ApJ, 724, 878
Tran K.-V. H. et al., 2010, ApJ, 719, L126
Umeda K. et al., 2004, ApJ, 601, 805
Velliscig M., van Daalen M. P., Schaye J., McCarthy I. G., Cacciato M., Le Brun A. M. C., Dalla Vecchia C., 2014, MNRAS, 442, 2641
Verde L., Matarrese S., 2009, ApJ, 706, L91
Vikhlinin A. et al., 2009, ApJ, 692, 1060
Vogelsberger M. et al., 2014, MNRAS, 444, 1518
von der Linden A. et al., 2014, MNRAS, 439, 2
Wang Y., 2014, Commun. Theor. Phys., 62, 109
Wang L., Steinhardt P. J., 1998, ApJ, 508, 483
Watson W. A., Iliev I. T., D'Aloisio A., Knebe A., Shapiro P. R., Yepes G., 2013, MNRAS, 433, 1230
Weller J., Battye R. A., Kneissl R., 2002, Phys. Rev. Lett., 88, 231301
Wen Z. L., Han J. L., 2015, ApJ, 807, 178
Wetterich C., 2004, Phys. Lett. B, 594, 17
Yang G. et al., 2014, ApJS, 215, 27
Ziparo F. et al., 2014, MNRAS, 437, 458

APPENDIX A: THE *EUCLID* SPECTROSCOPIC SURVEY

We use a procedure similar to the one described in Section 2 to determine the number of spectroscopic cluster galaxies within $r_{200,c}$, as a function of both cluster mass and redshift. Since the *Euclid* spectroscopic survey is flux limited in the Hα line, we consider the cluster Hα LF. There are not many determinations of the cluster Hα LF in the literature. We use the results of Iglesias-Páramo et al. (2002, for two nearby clusters, $z = 0.02$), Balogh et al. (2002, for a $z = 0.18$ rich cluster), Umeda et al. (2004, for a $z = 0.25$ cluster), and Kodama et al. (2004, for a $z = 0.4$ cluster).

The redshift evolution of the cluster Hα LF is (at best) poorly constrained, hence we have to make several assumptions for its three parameters, the characteristic luminosity $L^\star$, the normalization $\phi^\star$, and the faint-end slope α. We consider two possible evolutions. In the first, we assume the z-evolution of $L^\star$ to be the same as the one measured for the field Hα LF, i.e. $L^\star \propto (1+z)^{3.1}$ for $z \leq 1.3$, and no further evolution at higher redshift (Geach et al. 2010). In the second, we allow $L^\star$ to evolve at $z > 1.3$ with the same z-dependence established at lower redshifts. The second scenario is based on the idea that the preferred sites for galaxy star formation tends to shift to higher density regions at higher redshifts (Elbaz et al. 2007), even if the redshift at which this shift occurs is not well constrained (Ziparo et al. 2014).

The different cluster LFs we consider have been determined for different overdensities, Δ. To evaluate the $\Delta = 200$ value of $L^\star$ at $z = 0$, we perform a regression analysis between $\log[L^\star/(1+z_c)^{3.1}]$ and $\log\Delta$. We find $L^\star_{z=0} = 3.8 \times 10^{41}$ erg s^{-1}. Similarly to what we did in Section 2 for the K_s LF, we assume $\phi^\star \propto H^2(z)$. We then take the average of the $\phi^\star$ values obtained for the different clusters, after rescaling them for the factor $200\,H_0/[\Delta H(z)]$, and find $\phi^\star_{z=0} = 1.1$ Mpc^{-3}. As for α, we fix it to the value -0.7 obtained for the two nearby clusters by Iglesias-Páramo et al. (2002), since the other clusters observations were not deep enough to constrain the Hα LF faint end.

We convert the Hα luminosities into fluxes using $f_{H\alpha} = L_{H\alpha}/(2 \times 4\pi D^2_{L,c})$, where $D_{L,c}$ is the cluster luminosity distance and the factor $1/2$ accounts for the average dust extinction (Kodama et al. 2004). By integrating the LF down to the flux limit

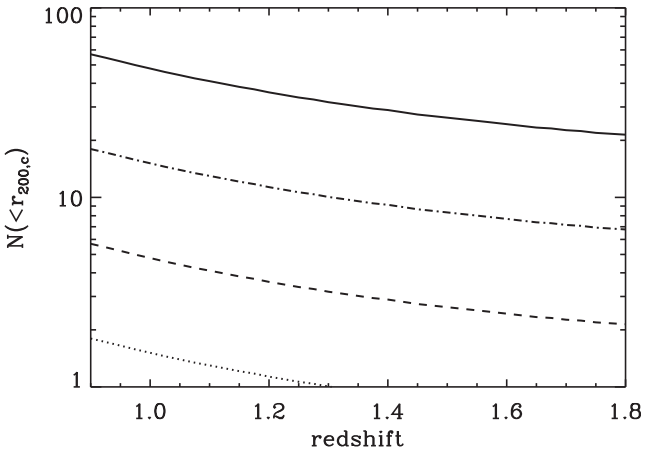

Figure A1. Number of cluster galaxies with spectroscopic redshifts within $r_{200,c}$ expected in the *Euclid* survey, as a function of redshift for clusters of different masses, $\log(M_{200,c}/M_{\odot}) = 15.0, 14.5, 14.0, 13.5$, solid, dot–dashed, dashed, dotted lines, respectively. These numbers are for the case of an evolving Hα luminosity function also beyond $z = 1.3$, i.e. they correspond to the solid blue curve in Fig. A2 (top panel).

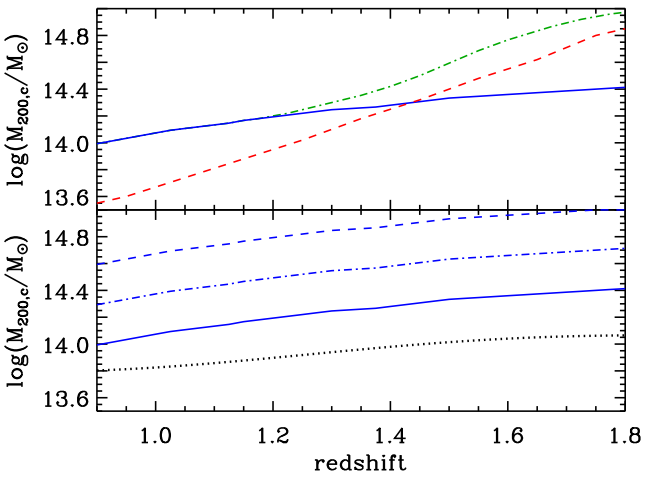

Figure A2. Selection function for the *Euclid* spectroscopic survey. In the top panel the solid blue curve indicates the selection function for clusters with five galaxies with measured spectroscopic redshift within $r_{200,c}$. This curve depends on the assumption that $L^{\star}$ continues to evolve beyond $z = 1.3$ following the same evolution law determined by Geach et al. (2010) for lower z. The dash–dotted curve depends instead on the assumption that there is no further evolution of $L^{\star}$ beyond $z = 1.3$, consistently with what is observed for the field Hα LF (Geach et al. 2010). The dashed red curve is an independent estimate based on the number densities of Hα field galaxies per redshift bin, estimated by Pozzetti et al. (2016). In the lower panel the solid, dash–dotted, and dashed lines show results for clusters with at least 5, 10, and 20 galaxies, respectively, with measured spectroscopic redshift within $r_{200,c}$, based on the assumption that $L^{\star}$ continues to evolve beyond $z = 1.3$. The dotted line is the selection function for the *Euclid* photometric survey (from Fig. 2), shown as a reference.

of the *Euclid* spectroscopic survey (3×10^{-16} erg s^{-1} cm^{-2}), we finally obtain the expected number density of galaxies within $r_{200,c}$. By multiplying the number density of galaxies within $r_{200,c}$ by the volume of the sphere of radius $r_{200,c}$, we obtain the number of galaxies in a cluster with Hα flux above the *Euclid* survey limit. Finally, we multiply this number by the expected completeness of the spectroscopic survey, ∼80 per cent.

In Fig. A1 we show the resulting estimates of the number of cluster galaxies with spectroscopic redshifts within $r_{200,c}$, as a function of redshift for clusters of different masses, for the case of an evolving Hα LF beyond $z = 1.3$. Note that only the redshift range 0.9–1.8 is shown, since this is the detectability range of the Hα line in the *Euclid* survey, according to the current design baseline.[9]

We also consider the following independent estimate of the cluster selection function in the *Euclid* spectroscopic survey. We use Pozzetti et al. (2016) estimates of the number densities of Hα emitting field galaxies per square degree and redshift bin that we convert to volume densities, $n_{\rm fd}$. To estimate the expected number density of Hα emitting galaxies in a cluster, we used $n_{\rm cl} = n_{\rm fd} b(z) \Delta \rho_{\rm c}/\rho_{\rm m}$, where $\rho_{\rm c}$ is the critical density and $\rho_{\rm m}$ the mass density of the Universe at any given redshift, Δ is the overdensity we want to sample in the cluster, and $b(z)$ is the redshift-dependent bias parameter that accounts for the different distribution of Hα galaxies and the underlying matter distribution. Taking $\Delta = 200$, the number of Hα galaxies in a cluster of mass $M_{200,c}$ is $N(\leq r_{200,c}) = (4\pi/3) r^3_{200,c} n_{\rm cl}$. We estimate the bias $b(z)$ from the comparison of the real-space correlation functions of matter and Hα galaxies, $b = (r_{0g}/r_{0m})^{-\gamma/2}$, where γ is the slope of the correlation function. We use the correlation lengths of the diffuse matter in our adopted cosmology, and those of Hα galaxies with luminosities corresponding to the *Euclid* flux limit at any given redshift (taken from Sobral et al. 2010). We estimate $b(z = 0.9) = 1.9$ and $b(z = 2.0) = 3.5$, and interpolate $b(z)$ between these two values at any redshift in the range 0.9–2.0.

[9] See the '*Euclid* GC Interim Science Review' by Guzzo & Percival, at http://internal.euclid-ec.org/?page_id=714. Access restricted to the *Euclid* Consortium members.

In Fig. A2, we show the limiting mass $M_{200,c}$ of a cluster with at least N_z galaxies with measured spectroscopic redshift within $r_{200,c}$ as a function of the cluster redshift. This is the selection function of clusters in the *Euclid* spectroscopic survey, in the sense that N_z concordant redshifts within a region of typical cluster size (i.e. $r_{200,c}$) are required to identify a cluster. The three different estimates of the spectroscopic selection function for clusters in the *Euclid* survey are rather different, and this reflects the current systematic uncertainties. From Fig. A2 (bottom panel), one can see that the spectroscopic survey selection function is above the photometric survey selection function. Hence, it will prove less efficient to search for clusters in the *Euclid* spectroscopic survey than in the photometric survey. Data from the spectroscopic survey will still be useful to confirm clusters detected in the photometric survey, thus improving the reliability of the sample.

APPENDIX B: CLUSTER MASS CALIBRATION

The impact of nuisance parameters on cosmological constraints from *Euclid* photometric clusters is going to be quite significant. This is especially true for the parameters directly related to the growth of structure history like the matter PS normalization σ_8, and for the CLP DE parameter w_a, that is particularly sensitive to the level of knowledge of the scaling relation evolution. In Fig. B1, we show how the cosmological constraints on the DE equation of state depend on our knowledge of the scaling relation. In particular, we show that strong constraints on the evolution of the scatter and the mass bias, allow to greatly improve the constraints on the DE EoS parameters. On the other hand, precise knowledge of these parameters at $z = 0$ is not of crucial importance, as shown by the

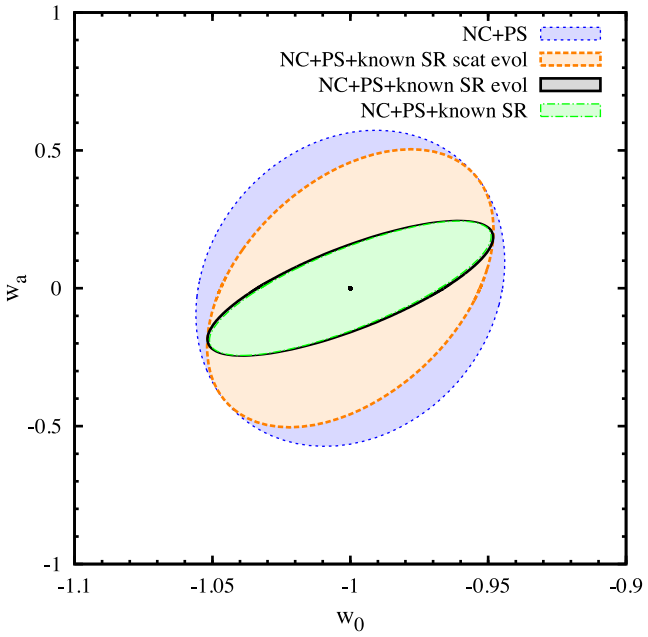

Figure B1. Constraints at the 68 per cent c.l. in the w_a–w_0 parameter plane. We show forecasts for the $N_{500,c}/\sigma_{\rm field} \geq 3$ *Euclid* photometric cluster survey obtained by (i) combining the FM information for number counts and power spectrum (NC+PS; blue dotted contour), (ii) same as (i) but assuming perfect knowledge of the evolution of the scatter (see equation (27); orange dashed contour); (iii) same as (i) but assuming perfect knowledge of the evolution of both the scatter and the bias (black solid contour); (iv) same as (i) but assuming perfect knowledge of all the four nuisance parameters (green dash–dotted contour). The blue and green curves are the same of Fig. 4, right-hand panel. Note that the solid black and the green dashed ellipses are almost coincident.

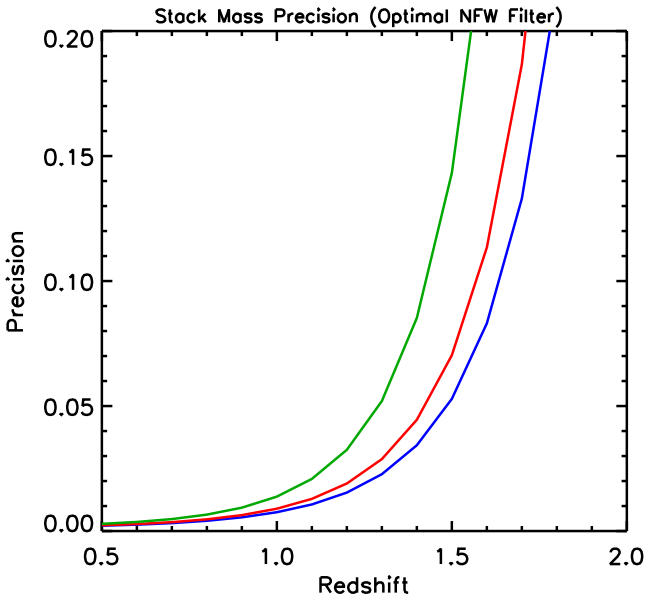

Figure B2. Calibrating cluster masses with gravitational shear. The curves show the expected precision on the mean mass of clusters in bins of $\Delta \log M_{200,c} = 0.2$ and $\Delta z = 0.1$, centred on masses (from top to bottom) of $M_{200,c} = 3 \times 10^{14}\,{\rm M}_\odot$ (green curve), $2 \times 10^{14}\,{\rm M}_\odot$ (red), and $1.5 \times 10^{14}\,{\rm M}_\odot$ (blue). We assume a lensing survey of 15 000 deg^2, the Tinker mass function in the base ΛCDM *Planck*cosmology, and shape noise with $\sigma = 0.3$.

overlapping constraints in the w_0, w_a plane in the figure (solid black and dashed green ellipses).

To maximize the scientific return of the *Euclid* galaxy cluster catalogue, it is therefore very important to know the mass scaling relation in an as much as possible precise and unbiased way. There are two avenues to obtain this goal. The first one is to cross-correlate the *Euclid* cluster sample with samples obtained at different wavelengths by different surveys. For instance, by the time *Euclid* will fly, the eROSITA full-sky X-ray cluster catalogue will be available, and will provide an important contribution to the cluster true mass estimation. Other useful cluster catalogues will include the SZ samples provided by the SPT, the ACT, and *Planck*.

The second avenue, which represents the strength of the *Euclid* mission, consists in exploiting internal *Euclid* data. Many photometrically selected clusters will appear as signal-to-noise ratio peaks in the *Euclid* full-sky cosmic shear maps. This weak gravitational lensing signal will permit us to estimate the cluster masses without relying on assumptions about dynamical equilibrium. Although only the more massive systems will permit individual mass measurements, we can nevertheless statistically calibrate the normalization of the cluster scaling relations down to the lowest masses in the catalogue by stacking. An example is given in Fig. B2, showing the level of precision expected on the mean mass of stacked clusters.

We first measure the mass of individual clusters with a matched filter, assuming that the mass density profile of all clusters follows an NFW profile. We then calculate the uncertainty on the mean mass of the individual measurements in bins of mass ($\Delta \log M_{200,c} = 0.2$) and redshift ($\Delta z = 0.1$). This result depends on the number of clusters expected in each bin, and for this purpose we have adopted the *Planck* cosmology (Planck Collaboration XVI 2014) and a *Euclid* survey of 15 000 deg^2. The figure only accounts for shape noise, with $\sigma = 0.3$.

The three curves trace the precision on the mean for mass bins centred at $M_{200,c} = 3 \times 10^{14}, 2 \times 10^{14}$, and $1.5 \times 10^{14}\,{\rm M}_\odot$ (from top to bottom) as a function of redshift. We do better on the lower mass systems because their larger number compensates for their lower individual signal-to-noise ratio measurements. The figure demonstrates that *Euclid* has the potential to calibrate the mean mass, and hence scaling relations, to 1 per cent out to redshift unity, and to 10 per cent out to $z \lesssim 1.6$ for clusters of $M_{200,c} = 1.5 \times 10^{14}\,{\rm M}_\odot$.

At the same time, the spectroscopic part of the *Euclid* survey will provide velocities for a few cluster members in each cluster detected with photometric data. Stacking these velocities for many clusters in bins of richness and redshift will allow a precise calibration of the velocity dispersion versus richness relation, and from this of the mass–richness relation.

In Fig. B3, we show the number of spectroscopic cluster members that will be available for stacks of clusters of given mass in bins of $\Delta z = 0.1$ and $\Delta \log M_{200,c} = 0.2$ (even if, in reality, the stacking procedure will be based on mass proxies, such as richness). These numbers are evaluated using the spectroscopic selection function (bottom panel of Fig. A2), and the expected number of clusters above a given mass in our adopted cosmology, by considering only clusters with at least five members with redshifts. In the figure we show the predictions for three cluster masses, $\log M_{200,c}/{\rm M}_\odot = 14.2, 14.4, 14.6$. The curve for $\log M_{200,c}/{\rm M}_\odot = 14.2$ is limited to $z \leq 1.25$ because of our choice of considering only clusters with $N_z \geq 5$. Note that the curve for $\log M_{200,c}/{\rm M}_\odot = 14.0$ (not shown) would be limited to $z \leq 1$ (and it would be lie in between those for 14.2 and 14.4).

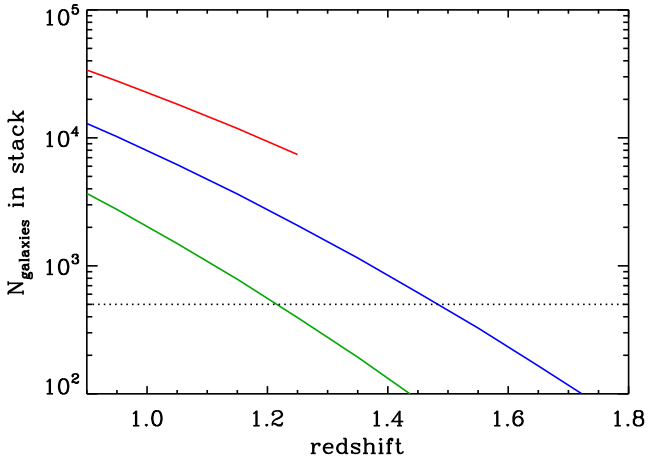

Figure B3. Calibrating cluster masses with spectroscopy. The curves show the number of cluster galaxies with redshifts available in stacks of clusters in bins of $\Delta \log M = 0.2$ and $\Delta z = 0.1$, as a function of redshift, for central values of the mass bins of $\log M_{200,c}/\mathrm{M}_\odot = 14.2$, 14.4, 14.6 (red, blue, green curves, respectively). The estimate is done only for clusters with a mass limit above that required for a minimum of five members with redshift – see Fig. A2, bottom panel. This requirement restricts the curve for $\log M/\mathrm{M}_\odot = 14.2$ to $z \leq 1.25$. The dotted line shows the value of 500 galaxies as a reference.

From the analysis of Biviano et al. (2006) we find that the statistical noise in the velocity dispersion estimate of a sample of ∼500 cluster members is ∼9 per cent, which translates into a ∼27 per cent statistical noise in the mass estimate. A similar figure has been obtained by Mamon, Biviano & Boué (2013) when using the full velocity distribution to constrain cluster masses. The value of 500 is displayed in Fig. B3, and it shows that a very precise spectroscopic calibration of cluster masses will be possible for stacks of clusters with $14.2 \leq \log M_{200,c}/\mathrm{M}_\odot \leq 14.6$ over the redshift range $0.9 \leq z \leq 1.2$, and even beyond that ($z \lesssim 1.5$) for clusters with masses $\log M_{200,c}/\mathrm{M}_\odot \simeq 14.4$. Spectroscopic calibration of cluster masses at higher redshifts will be feasible with reduced precision, but lack of statistics will hamper cluster mass calibration at $\log M_{200,c}/\mathrm{M}_\odot < 14.2$.

Potential worries that we have not addressed in these estimates are contamination and fragmentation. We have argued in Section 2 that contamination by projection effects is not a dominant effect, even at high redshifts. Fragmentation occurs when a real large cluster is broken into smaller subunits by the cluster identification algorithm. This could affect the velocity dispersion versus richness calibration, since the former is less affected by the fragmentation effect than the latter. To keep the fragmentation issue under control, the *Euclid* collaboration will use a battery of sophisticated, independent cluster finder algorithms.

The wide *Euclid* survey will allow precise calibration of the mass–observable relation out to $z \lesssim 1.6$, using gravitational lensing and spectroscopy. The deep *Euclid* survey will allow to extend this calibration to even higher redshifts, although with a much more limited statistics on the number of clusters. Overall, by combining *Euclid* internal mass calibration with the cross-correlation with external SZ and X-ray surveys, we should be able to significantly mitigate the degrading effect of the nuisance parameters on cosmological constraints.

This paper has been typeset from a TEX/LATEX file prepared by the author.